https://doi.org/10.5194/egusphere-2026-7095
Preprint. Discussion started: 27 November 2026
© Author(s) 2026. CC BY 4.0 License.

Projected Alpine precipitation changes across weather regimes in regional climate simulations

Ian Castellanos[1], Martin Ménégoz[1], Juliette Blanchet[1], Julien Beaumet[2], Sara Bacer[3], Eduardo Moreno-Chamarro[4,a], Mondher Chekki[1], Xavier Fettweis[5]

[1]Univ. Grenoble Alpes, CNRS, INRAE, IRD, Grenoble INP, IGE, 38000 Grenoble, France
[2]Atmo Auvergne-Rhône-Alpes, France
[3]Max Planck Institute for Chemistry, Mainz, Germany
[4]Barcelona Supercomputing Center (BSC), Barcelona, Spain
[a]Now at: Max Planck Institute for Meteorology, Hamburg, Germany
[5]Department of Geography, University of Liege, Liege, Belgium

Correspondence to: Ian Castellanos (ian.castellanos-dupuy@univ-grenoble-alpes.fr)

Abstract. The Alps lie at the intersection of major large-scale climate influences, making precipitation changes in the region particularly sensitive to atmospheric circulation. Because global climate models (GCMs) poorly resolve Alpine topography, regional downscaling is required to represent precipitation patterns and their response to climate change. This study investigates the relationship between large-scale circulation and Alpine precipitation using weather regimes (WRs) over the North Atlantic-European sector. Weather regimes are identified in the ERA5 reanalysis and in two GCMs, MPI-ESM1-2-HR and EC-Earth3, using a weather type decomposition methodology based on principal component analysis and k-means clustering of the geopotential height at 500hPa. The resulting circulation patterns are linked to precipitation simulated by the regional climate model MAR, driven by ERA5 and by the two GCMs. Both GCMs reproduce the canonical North Atlantic-European weather regimes with sufficient fidelity to allow a one-to-one comparison with ERA5, although circulation biases remain and are reflected in the downscaled precipitation patterns. Projected circulation changes between 1961-2009 and 2050-2099 reveal heterogeneous responses across weather regimes, models, and scenarios, with no consistent circulation response emerging across all simulations. Changes in WR frequency and persistence are generally limited and non-significant. Differences between realizations of the same model can be comparable in magnitude to differences between models, suggesting that internal variability remains a major source of uncertainty in future circulation projections. Projected winter precipitation changes are generally weak and not statistically significant when averaged over the season. However, substantially larger and often significant changes emerge when precipitation is analysed separately for individual weather regimes, as opposing responses can compensate for one another in seasonal averages. Summer responses are generally more pronounced, particularly in the MPI-driven simulations, which project widespread precipitation decreases associated with NAO- and Atlantic Ridge conditions. These results demonstrate the value of a weather-regime framework for investigating future precipitation changes at middle latitudes, and especially in complex mountain regions. They highlight the importance of accurately representing large-scale circulation in climate projections and suggest that analyses based solely on seasonal mean precipitation may overlook important circulation-dependent responses to climate change. The diversity of responses

https://doi.org/10.5194/egusphere-2026-7095
Preprint. Discussion started: 27 November 2026
© Author(s) 2026. CC BY 4.0 License.

across regimes and scenarios further suggests that future Alpine precipitation changes arise from a complex interplay between circulation changes and thermodynamic effects that need to be further explored.

1 Introduction

The Alps constitute the dominant orographic feature of western Europe and are located at the crossroads of major large-scale climate influences. The Alpine ridge forms a pronounced climatic boundary, separating the region into northern and southern sectors with distinct precipitation regimes: the northern Alps are primarily influenced by temperate westerlies, whereas the southern Alps are subject to a more Mediterranean climate (Brunetti et al., 2006). Observational studies generally report increasing precipitation trends in the northern Alps and decreasing trends in the southern Alps, although their magnitude and significance vary depending on season and temporal scale (e.g. Schmidli et al., 2002; Auer et al., 2007; Masson and Frei, 2016). In contrast, trends in extreme precipitation are typically found to increase across most of the Alpine region, broadly consistent with the thermodynamic relationship linking atmospheric warming and moisture availability described by the Clausius-Clapeyron relationship (Ban et al., 2015; Brönnimann et al., 2018; Ménégoz et al., 2020). Nevertheless, changes in large-scale circulation can substantially modulate these trends, leading to pronounced seasonal and regional contrasts in extreme precipitation in the Alps (Blanchet et al., 2021a).

Climate projections suggest that north-south contrasts in precipitation are likely to persist under future warming, although the location of the transition zone is expected to vary seasonally. In summer, projections generally indicate a northward shift of this transition, placing much of the Alpine region within the drying tendency projected over southern Europe and the Mediterranean basin (Coppola et al., 2020; de Vries et al., 2022). In contrast, winter projections locate the transition closer to the latitude of the Alps, resulting in more heterogeneous precipitation responses across the region (Coppola et al., 2020). These contrasted and seasonally dependent responses further highlight the complexity of assessing future precipitation changes in the Alps.

A major source of this complexity lies in the strong dependence of Alpine precipitation on large-scale atmospheric circulation (Wanner et al., 1997; Plaut and Simonnet, 2001; Quadrelli et al., 2001; Efthymiadis et al., 2007; Blanc et al., 2022). The Alpine topography acts as a barrier to mid-tropospheric flow, enhancing orographic precipitation (Napoli et al., 2019) in response to synoptic-scale circulation patterns. Variability and trends in extreme precipitation have likewise been linked to large-scale circulation (Blanchet et al., 2021a, 2021b).

A common framework for describing atmospheric circulation variability is provided by weather regimes, which correspond to recurrent and quasi-stationary states of the atmosphere. Beyond their usefulness as a statistical framework for investigating links between circulation and regional climate, weather regimes also represent physically meaningful modes of atmospheric variability (Hochman et al., 2021), making them valuable for both climate diagnostics and weather prediction (e.g., Lavaysse et al., 2018; Cortesi et al., 2021).

https://doi.org/10.5194/egusphere-2026-7095
Preprint. Discussion started: 27 November 2026
© Author(s) 2026. CC BY 4.0 License.

Global climate models (GCMs) reproduce large-scale circulation over the North Atlantic-European region (also commonly referred to as the Euro-Atlantic region) with varying degrees of skill (Hertig and Jacobeit, 2014). Biases in the representation of individual weather regimes may therefore propagate into regional climate simulations and contribute to errors in projected precipitation changes (Evin et al., 2021). More fundamentally, analyses based solely on seasonal means may mask contrasting responses associated with different circulation patterns, as increases and decreases occurring under distinct weather regimes can compensate for one another. Examining precipitation conditionally on weather regimes therefore provides a process-based framework for interpreting precipitation variability and change, while also allowing the influence of circulation biases in GCMs to be assessed.

In this study, we focus on two state-of-the-art GCMs, EC-Earth3 and MPI-ESM1-2-HR. Their relatively high spatial resolution and advanced physical parameterizations enable a realistic representation of synoptic-scale circulation over Europe, which is essential for weather regime identification. Nevertheless, their resolution remains insufficient to explicitly resolve Alpine topography, motivating the use of regional downscaling with the model MAR (Modèle Atmosphérique Régional). Considering two GCMs and their corresponding regional climate simulations allows us to assess the consistency of circulation-precipitation relationships across different model configurations and to identify responses that are common to, or differ between, the simulations. The limited number of GCMs, however, does not allow a comprehensive assessment of projection uncertainty.

The remainder of the paper is organized as follows. Section 2 presents the datasets and methods, including the weather regime classification and precipitation analysis framework. Section 3 examines the results by first evaluating the historical climatology of large-scale circulation and associated precipitation patterns, and then investigating projected changes and their relationship to weather regime variability. Section 4 provides a discussion of the results as well as a final conclusion.

2 Data and methods

2.1 Model data

2.1.1 General circulation models

This study employs two state-of-the-art global climate models (GCMs) from Phase 6 of the Coupled Model Intercomparison Project (CMIP6; Eyring et al., 2016): MPI-ESM1-2-HR and EC-Earth3. These models are used both to classify the large-scale circulation over the North Atlantic-European region into weather regimes and to provide lateral boundary conditions for MAR simulations over the Alps.

The two GCMs were selected for their demonstrated ability to realistically reproduce key aspects of the North Atlantic-European climate system. In particular, they show good skill in representing large-scale atmospheric circulation, mid-tropospheric geopotential height patterns, and sea-surface temperatures over the North Atlantic-European sector (Castellanos

https://doi.org/10.5194/egusphere-2026-7095
Preprint. Discussion started: 27 November 2026
© Author(s) 2026. CC BY 4.0 License.

et al., 2026). More broadly, several CMIP6 model evaluations have identified MPI-ESM1-2-HR and EC-Earth3 among the better-performing models for the representation of European and North Atlantic climate variability. Both models have been shown to reproduce sea-level pressure patterns (Cannon, 2020), synoptic-scale circulation regimes (Fernández-Granja et al., 2021, for MPI-ESM1-2-LR and EC-Earth3), and Mediterranean wind distributions (Çalışır et al., 2026) with good fidelity when compared to reanalysis products.

Particularly relevant to the present study, Fabiano et al. (2020) showed that both models provide a realistic representation of the four North Atlantic-European weather regimes examined here. This makes them especially suitable for investigating the links between large-scale circulation and Alpine precipitation. Although both models perform well overall, EC-Earth3 is frequently identified as one of the most skillful CMIP6 models for the representation of North Atlantic-European circulation, while MPI-ESM1-2-HR also consistently ranks among the better-performing models in this regard.

MPI-ESM1-2-HR

MPI-ESM1-2-HR is the high-resolution configuration of the Max Planck Institute Earth System Model, developed for CMIP6 applications. To provide a comprehensive representation of the climate system, it couples the following components :

- the atmospheric model ECHAM6.3 (Stevens et al., 2013; Mauritsen et al., 2019),
- the MPIOM ocean model (Jungclaus et al., 2013),
- an ocean and land carbon cycle, the Hamburg Model of the Ocean Carbon Cycle (HAMOCC; Ilyina et al., 2013; Paulsen et al., 2017) and the land surface scheme JSBACH (Reick et al., 2013).

The oceanic and atmospheric components are coupled through the OASIS3-MCT coupler (Craig et al., 2017). The atmospheric component operates at a relatively high horizontal resolution (T127, ~100 km) with 95 vertical levels extending into the upper stratosphere, allowing for an improved simulation of large-scale circulation features and stratosphere-troposphere interactions with respect to the lower resolution configuration MPI-ESM1-2-LR (Müller et al., 2018). A 10-member ensemble of MPI-ESM1-2-HR simulations is available (Olonscheck et al., 2023).

Compared to lower-resolution configurations, MPI-ESM1-2-HR provides an improved representation of atmospheric variability and extremes, although, as with most GCMs, biases remain in regional precipitation and circulation patterns (Müller et al., 2018). Additionally, it has been previously selected to drive regional simulations over Italy in Struglia et al. (2025), owing in part to its well-balanced radiation budget.

EC-Earth3

EC-Earth is a European consortium of national meteorological services and research institutes started in 2006. It has developed successive generations of a fully coupled Earth system model (ESM) of the same name. EC-Earth3

https://doi.org/10.5194/egusphere-2026-7095
Preprint. Discussion started: 27 November 2026
© Author(s) 2026. CC BY 4.0 License.

is the generation of the model used in the CMIP6 database (Döscher et al, 2022). Its standard configuration consists of several interacting components :

- the atmosphere component is based on the Integrated Forecast System (IFS) CY36R4 of the European Centre for Medium-Range Weather Forecasts (ECMWF) which is extensively documented at https://www.ecmwf.int/en/publications/ifs-documentation (last access: 12 October 2026),
- the land surface component is the Hydrology Tiled ECMWF Scheme of Surface Exchanges over Land (HTESSEL; van den Hurk et al., 2000; Balsamo et al., 2009; Dutra et al., 2010; Boussetta et al., 2013),
- the ocean component is the Nucleus for European Modelling of the Ocean (NEMO; Madec and the NEMO team, 2008; Madec et al., 2015).

These components are coupled through the OASIS3-MCT coupler (Craig et al., 2017). The atmosphere component has a high resolution of ~80 km with 91 vertical levels (T255L91).
Additionally, it has been used by Rivosecchi et al. (2024) to study the impact of weather regimes on Mediterranean precipitation, owing to its good skill in simulating the North-Atlantic Oscillation (NAO) and its relationship with mean and extreme precipitation.

2.1.2 ERA5

ERA5 is the fifth generation atmospheric reanalysis produced by the European Centre for Medium-Range Weather Forecasts (ECMWF). It provides a global, gridded reconstruction of the atmospheric state from 1940 to the present at high spatial and temporal resolution. In this study, ERA5 serves as the reference dataset for large-scale circulation and weather regime identification. It is also used to drive MAR, providing a benchmark against which the GCM-driven MAR simulations can be evaluated.

ERA5 is provided as a 10-member ensemble designed to estimate uncertainties associated with the observations and data assimilation procedure; only the ensemble mean is used in this study. Because observations are assimilated into the reanalysis, the ERA5 ensemble is constrained to follow the observed evolution of the atmosphere. Its ensemble spread therefore represents uncertainty in the reconstructed atmospheric state rather than internal climate variability. By contrast, ensemble members of a GCM are independent realizations subject to the same external forcing, and their spread primarily reflects internal climate variability. Such variability may account for part of the differences between individual GCM realizations and ERA5, particularly at interannual to decadal timescales. This distinction is especially important when evaluating large-scale circulation and weather regimes, whose spatial patterns and frequencies can vary substantially between realizations even under identical external forcing. The magnitude of this internal variability is illustrated in Appendix A using multiple realizations of MPI-ESM1-2-HR.

https://doi.org/10.5194/egusphere-2026-7095
Preprint. Discussion started: 27 November 2026
© Author(s) 2026. CC BY 4.0 License.

ERA5 is generated using the Integrated Forecasting System (IFS; cycle 41r2) and a state-of-the-art data assimilation framework that combines numerical weather prediction with a wide range of observations, including satellite measurements, radiosondes, and surface-based observations. The atmospheric component operates at a horizontal resolution of approximately 31 km with 137 vertical levels extending up to 0.01 hPa. Atmospheric observations are assimilated using an incremental four-dimensional variational (4D-Var) scheme (Hersbach et al., 2020).

Over Europe, ERA5 has been shown to realistically reproduce wind fields (Olauson, 2018; Molina et al., 2021; Laurila et al., 2021) which are related to the large-scale circulation. Although its spatial resolution remains insufficient to fully resolve the effects of complex topography on near-surface winds (Gutiérrez et al., 2024), the assimilation of extensive observational datasets makes ERA5 one of the most reliable representations of synoptic-scale atmospheric circulation currently available. Consequently, it provides a suitable reference for weather regime analysis and for driving regional climate simulations over the Alps to compare to GCM-driven simulations.

2.1.3 Modèle Atmosphérique Régional (MAR)

MAR is a regional climate model designed to simulate atmospheric processes and their interactions with the surface at a resolution ranging from 5 to 50km. It is based on the hydrostatic primitive equations and uses a terrain-following vertical coordinate (Gallée and Schayes, 1994 ; Gallée et al., 2005). It has been developed for polar regions (Gallée, 1995), but has been used in a variety of settings, including precipitation studies over Europe and the Alpine region (e.g. Doutreloup et al., 2019; Ménégoz et al., 2020). Owing to its fine spatial resolution and multi-layer snow scheme, MAR provides added value over complex terrain by improving the representation of precipitation, temperature, and snow-related processes (Beaumet et al., 2021).

In this study, MAR is driven laterally by the ERA5 reanalysis and by the GCMs EC-Earth3 and MPI-ESM1-2-HR. The simulations are centred over the Alps and use a domain extending from 1.5 to 18.5°E and 41.5 to 49.5°N (Figure 1), with a horizontal resolution of 7 km and 24 vertical levels extending up to 0.1 hPa. The simulations employed in this study were performed using either version 3.10 or version 3.14 of MAR and are summarized below:

- MAR version 3.10 driven by EC-Earth3 (historical, 1961-2014 ; SSP2-4.5, 2015-2100);
- MAR version 3.10 driven by MPI-ESM1-2-HR (historical, 1961-2014 ; SSP2-4.5, 2015-2100 ; SSP5-8.5, 2015-2100);
- MAR version 3.14 driven by ERA5 (1940-2025).

The CMIP6 simulations include a historical period spanning 1850-2014. However, due to computational constraints, only the period 1961-2014 was dynamically downscaled. Future projections cover the period 2015-2100 and include the intermediate-emission scenario SSP2-4.5 and the high-emission scenario SSP5-8.5 (O'Neill et al., 2016).

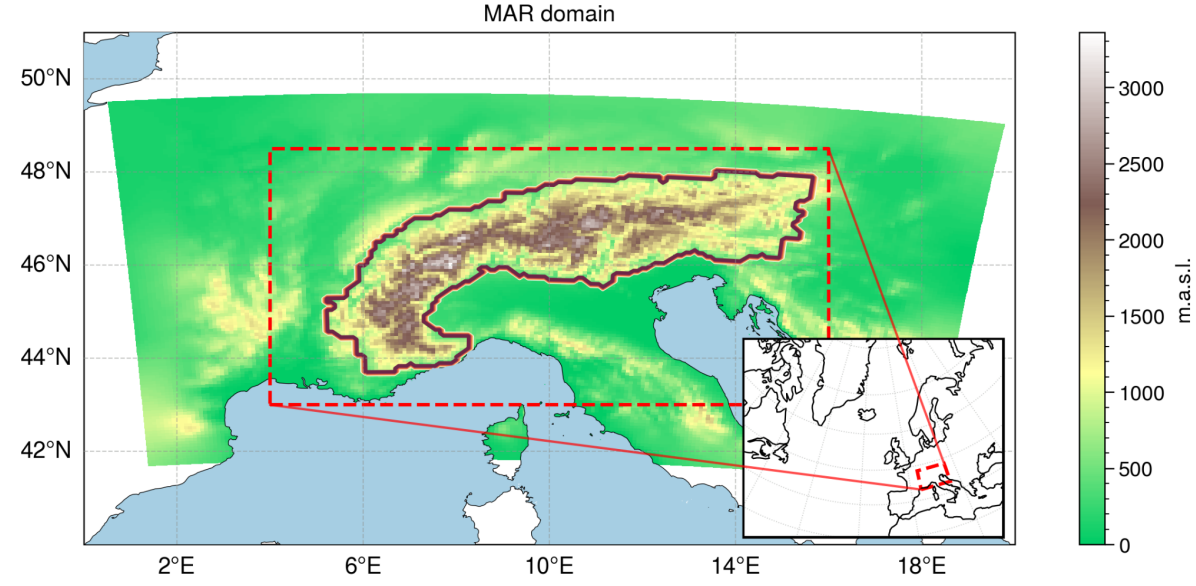
https://doi.org/10.5194/egusphere-2026-7095
Preprint. Discussion started: 27 November 2026
© Author(s) 2026. CC BY 4.0 License.

Because two versions of MAR are used in this study, their main differences are briefly summarized here. The primary distinction concerns the radiative transfer scheme. MAR version 3.10 employs the Morcrette radiation scheme (Morcrette, 1991; 2002), whereas version 3.14 uses the ecRad scheme (Hogan and Bozzo, 2018; Grailet, 2023). The two versions also differ in their treatment of aerosols. Version 3.10 uses a temporally evolving aerosol climatology until 2005, after which aerosol concentrations are fixed at their 2005 values. In contrast, version 3.14 relies on a fixed aerosol climatology derived from the European Centre for Medium-Range Weather Forecasts (ECMWF; cycle 43r3; Bozzo et al., 2020), which remains unchanged throughout the simulation period. This results in modest differences in the climatologies produced by the two model versions (see Castellanos et al., 2026, Appendix C therein), without leading to major differences in MAR's representation of the regional climate. Furthermore, precipitation over the Alps is primarily controlled by the large-scale atmospheric forcing and the representation of topography. Since both MAR configurations employ the same domain and horizontal resolution, the influence of the version change on precipitation is expected to remain secondary compared to that of the driving data.

An evaluation of MAR simulations driven by EC-Earth3 (v3.10) and MPI-ESM1-2-HR (v3.10 and v3.14) against the Alpine Precipitation Grid Dataset (APGD; Isotta et al., 2014) indicates a generally realistic representation of precipitation at elevations below 1500 m a.s.l. in all seasons except summer (Castellanos et al., 2026; Appendix C therein). At higher elevations, however, MAR exhibits a wet bias during winter, spring, and autumn, reaching approximately 7 mm day^{-1} in winter. Conversely, summer precipitation is underestimated across the elevation range, with dry biases locally exceeding 5 mm day^{-1}.

These biases are consistent with Beaumet et al. (2021). Using MAR driven by the ERA-20C reanalysis (Poli et al., 2016) and evaluated against the S2M snow and climate reanalysis dataset (Vernay et al., 2019), they also reported a good agreement at low elevations and an overestimation of precipitation at higher elevations. More generally, previous studies (e.g. Kotlarski et al., 2015; Matiu et al., 2024) identified an excessive precipitation-elevation gradient as a common bias among regional climate models over complex terrain.

https://doi.org/10.5194/egusphere-2026-7095
Preprint. Discussion started: 27 November 2026
© Author(s) 2026. CC BY 4.0 License.



225 **Figure 1: MAR topography and domain, with inset showing the approximate window for which large-scale circulation was computed (20-80 °N, -80-50 °E).**

2.2 Methods

2.2.1 Weather regime classification

In this study, we investigate how the large-scale weather regimes occurring in the GCM used to laterally force the MAR
230 regional simulation influence the precipitation patterns in the Alps. Following Bacer et al. (2022), the GCM data are first normalized and then classified into weather regimes over the North Atlantic-European area (domain depicted in the Figure 1 inset), using the Weather Type Decomposition (WTD) methodology (Michelangeli et al., 1995; Philipp et al., 2016).

Large-scale circulation is characterized using geopotential height at 500 hPa (Z500). Daily anomalies, hereafter ΔZ500, are computed as the deviation of daily Z500 from a reference climatology defined by the mean annual cycle over a 50-year
235 period (1960-2009 for the historical period and 2050-2099 for future projections). The analysis is performed independently for an extended winter season (November-December-January-February-March; NDJFM) and summer (June-July-August; JJA), with the same seasonal separation maintained throughout the subsequent classification procedure. The anomalies are then weighted by the square root of the cosine of latitude (Chung and Nigam, 1999) to account for the gridcell areas that vary with the latitude (e.g. Cassou, 2008). To ensure consistency across datasets, the anomalies are subsequently interpolated
240 onto a common 1° × 1° grid over a window spanning 20-80 °N and −80-50 °E.

The WTD methodology is then applied independently to each season and period in two steps. First, the dimensionality of the dataset is reduced using principal component analysis (PCA), following previous studies (e.g. Boé and Terray, 2008; Hertig and Jacobeit, 2014; Sáenz and Durán-Quesada, 2015). This step alleviates to an extent the curse of dimensionality associated

https://doi.org/10.5194/egusphere-2026-7095
Preprint. Discussion started: 27 November 2026
© Author(s) 2026. CC BY 4.0 License.

with the high-resolution geopotential height fields by removing redundant information and retaining only the dominant modes of variability. It also improves the efficiency and robustness of the subsequent k-means clustering by projecting the data onto a reduced set of orthogonal components. The leading modes explaining 95% of the total variance (24 components on average) are retained.

Second, k-means clustering is performed on the reduced dataset, with the number of clusters fixed to four. Each day within the corresponding season of the historical, SSP2-4.5, and SSP5-8.5 simulations is assigned to one of these clusters. In winter, these correspond to the canonical North Atlantic-European weather regimes (positive and negative NAO: NAO+ and NAO−; Atlantic Ridge; and Scandinavian Blocking, or simply Blocking), as in Cassou (2008), Ullmann et al. (2014), and Fabiano et al. (2020, 2021).

Four clusters are also retained for summer. The resulting regimes exhibit sufficient similarity to their winter counterparts to allow a one-to-one correspondence. This is consistent with previous studies that identified summer weather regimes comparable to the winter canonical ones over the North Atlantic-European region (e.g. Boé et al., 2009). Furthermore, Babanov et al. (2023) found k-means clustering to be among the most robust methods for identifying weather regimes and showed that it produces summer regimes that are particularly consistent with their winter counterparts.

To characterize the atmospheric flow associated with each weather regime, seasonal daily anomalies of wind velocity at 500 hPa are also computed, following the same procedure as for ΔZ500. These anomalies are used to describe the circulation patterns associated with each regime.

2.2.2 Climatologies and projected change estimations

We then analyze precipitation over the Alps as simulated by the limited-area model MAR. For each grid point, the mean daily precipitation is first computed separately for the historical (1961-2009) and future (2050-2099) periods for the extended winter (NDJFM) and summer (JJA) seasons, and expressed in millimeters water equivalent (mm w.e.). The same procedure is then applied to each weather regime by selecting the corresponding days identified using the WTD methodology (Sect. 2.2.1).

Precipitation anomalies associated with each weather regime are calculated as the difference between the regime-specific seasonal mean and the overall seasonal mean, normalized by the seasonal mean. This yields a relative anomaly expressed as a percentage, indicating the increase or decrease in precipitation for a given weather regime compared to climatological conditions.

Two spatial masks representing the northern and southern Alps are defined to describe precipitation variability over the Alps. First, grid points are selected based on two criteria: an elevation of at least 360 m above sea level (m a.s.l.) and the presence of at least one neighboring grid point with an elevation exceeding 1300 m a.s.l. (see the contour in Figure 1). These thresholds were chosen to accurately delineate the Alpine region while excluding other mountainous areas within the simulation domain.

https://doi.org/10.5194/egusphere-2026-7095
Preprint. Discussion started: 27 November 2026
© Author(s) 2026. CC BY 4.0 License.

Second, the north-south boundary is based on the climatological division proposed by Auer et al. (2007). The easternmost section of the boundary suggested by Auer et al. (2007) is slightly shifted northward to better follow the Alpine ridge, as this adjustment provides a more physically consistent separation for precipitation patterns (see the inner delimitation in Figs. 3-5, 9-11).

2.2.3 Evaluation of weather regime change with Teweles-Wobus score

The Teweles-Wobus score (Teweles and Wobus, 1954) quantifies differences in the spatial structure of a field. When applied to geopotential height, it provides a measure of dissimilarity that emphasizes the relative positioning of pressure systems rather than their absolute magnitude. In contrast to a Euclidean distance, which combines differences in both intensity and location, this metric isolates changes in the shape of the field. This distinction is particularly relevant, as the configuration of geopotential height governs wind direction, a key driver of regional precipitation patterns. For this reason, the Teweles-Wobus score has been widely used in atmospheric circulation analyses (e.g., Daoud et al., 2016; Blanc et al., 2022).

Following Blanc et al. (2022), the score between two days k and k' is defined as:

$$TWS_{k,k'} = \frac{\sum_{(j,j') \in Adj} \left| \left(z_j^k - z_{j'}^k \right) - \left(z_j^{k'} - z_{j'}^{k'} \right) \right|}{\sum_{(j,j') \in Adj} max\left(\left| \left(z_j^k - z_{j'}^k \right) - \left(z_j^{k'} - z_{j'}^{k'} \right) \right| \right)}$$

where Adj denotes the set of pairs of neighboring grid points in the zonal and meridional directions over the domain. The score thus represents a normalized aggregate of differences in horizontal geopotential height gradients between the two fields.

By construction, $TWS_{k,k'}=0$ indicates identical flow structures, while $TWS_{k,k'}=1$ corresponds to completely opposite gradient orientations. It should be noted, however, that relatively high scores may also arise from weakly structured (i.e., nearly flat) geopotential fields. In such cases, small absolute differences in gradients can lead to large normalized values, and therefore high scores do not necessarily imply strong dynamical contrasts.

In this study, the Teweles-Wobus score is used to quantify the change of the weather type fields between the historic period (1961-2009) and the projection (2050-2099) for a given model realisation.

2.2.4 Significance of regime frequency, precipitation, and persistence changes

To assess the statistical significance of projected changes in regime frequency, precipitation, and persistence, different approaches are applied depending on the statistical properties of each variable. Frequency is defined as the fraction of days that fall under a certain regime, while persistence is the average number of consecutive days that the regime stays in.

Regime frequency and precipitation

Significance in changes of regime frequency and spatially averaged precipitation is evaluated using an independent Student's *t*-test.

https://doi.org/10.5194/egusphere-2026-7095
Preprint. Discussion started: 27 November 2026
© Author(s) 2026. CC BY 4.0 License.

For regime frequency, the annual number of days associated with each weather regime is computed for both the historical and projected periods. The *t*-test is then applied to these two independent samples. Statistical significance is assessed at the $p < 0.05$ and $p < 0.10$ levels, corresponding to two confidence thresholds.

For precipitation, daily values are first spatially averaged over the region of interest (northern or southern Alps) after applying the corresponding mask, for the historical and projected periods separately. When relevant, data are further subset by weather regimes. The *t*-test is then performed between the historical and projected samples. Statistical significance is assessed at the $p < 0.05$ and $p < 0.10$ levels as well.

Regime persistence

Regime persistence does not follow a normal distribution; therefore, a parametric *t*-test is not appropriate. Instead, significance is assessed using a permutation (resampling) test.

The difference in persistence between the historical and projected periods is first computed. The two samples are then pooled and randomly resampled: a subset of size n1 (corresponding to the size of the historical sample) is drawn, and the remaining values form a second sample. The difference in mean persistence between these two resampled groups is calculated. This procedure is repeated 1000 times to generate an empirical distribution of differences under the null hypothesis of no change.

Significance is determined by comparing the observed difference to this distribution. Changes are considered significant at the 5% level if the observed difference falls outside the 2.5th-97.5th percentile range, and at the 10% level if it falls outside the 5th-95th percentile range.

3 Results

3.1 Historical climatologies

In this section, we examine the relationship between large-scale weather regimes in the GCMs and the regional precipitation patterns in the MAR experiment over the Alps, and establish the precipitation climatology for the period 1961-2009. The ERA5 reanalysis is used as a reference dataset to evaluate the performance of the GCMs, while the MAR simulation driven by ERA5 serves as a benchmark for comparison with MAR simulations driven by GCM outputs.

https://doi.org/10.5194/egusphere-2026-7095
Preprint. Discussion started: 27 November 2026
© Author(s) 2026. CC BY 4.0 License.

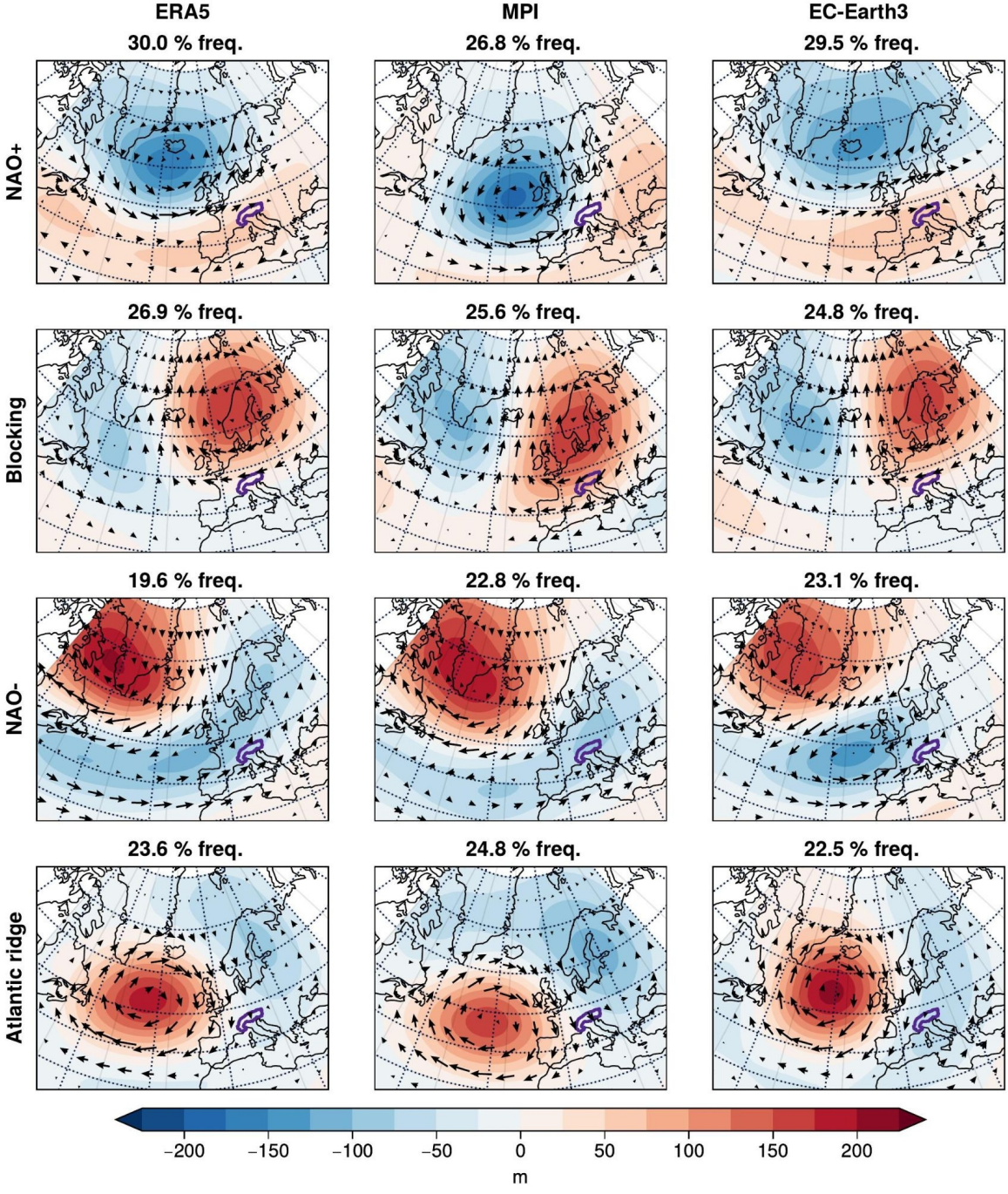


Figure 2: Geopotential height and winds at 500hPa for winter (NDJFM), 1961-2009. Purple contour shows the Alps. Left: ERA5 reanalysis; middle: MPI-ESM1-2-HR experiment (r1i1p1f1); right: EC-Earth3 experiment (r25i1p1f1). Rows correspond to the four weather regimes identified in Sect.2.2.1.

https://doi.org/10.5194/egusphere-2026-7095
Preprint. Discussion started: 27 November 2026
© Author(s) 2026. CC BY 4.0 License.

The spatial maps presented in this section focus on winter conditions (NDJFM). Equivalent diagnostics for summer (JJA) are provided in Appendix A, while seasonal statistics for both winter and summer weather regimes are reported in Tabs. 1 and 2.

Figure 2 presents the four winter weather regimes and their frequencies for ERA5, MPI-ESM1-2-HR (hereafter MPI), and EC-Earth3. Both GCMs were selected for their demonstrated ability to represent large-scale circulation over the North Atlantic-European region, and accordingly reproduce the four regimes with relatively good fidelity (see Sect. 2.1.1). Nevertheless, some ambiguity remains in the interpretation of individual regimes. In particular, the MPI counterpart of the NAO+ regime could arguably be interpreted as an inverse Atlantic Ridge regime. It is classified as NAO+ in the present study to maintain consistency with both the ERA5 classification and previous weather-regime literature. A brief analysis of weather-regime variability across ten MPI realizations is provided in Appendix A.

Because ERA5 and the GCM simulations represent different realizations of the climate system, discrepancies between the simulations and ERA5 may arise both from model biases and from internal climate variability. While these differences are described below, their attribution is not investigated further in this study.

For NAO+, the cyclonic center of action in MPI is displaced southward relative to ERA5, whereas in EC-Earth3 it is shifted slightly northward. As a result, the flow over the Alps remains predominantly westerly in ERA5 and EC-Earth3 but becomes southwesterly in MPI.

The Blocking regime exhibits an anticyclonic center in MPI which is displaced southward, resulting in northeasterly rather than easterly flow over the Alps. For the NAO- regime, the ridge is shifted slightly eastward in MPI, while in EC-Earth3 its extension into the Atlantic is reduced. Nevertheless, EC-Earth3 remains closer to ERA5 in terms of the associated flow over the Alpine region. Finally, the Atlantic Ridge regime is characterized by a latitudinal bias in both models, with a southward displacement in MPI and a northward extension in EC-Earth3.

Additional metrics describing weather-regime behaviour are provided in Tabs. 1 and 2 for winter (NDJFM) and summer (JJA), respectively. These include regime frequency, defined as the fraction of days assigned to a given regime within a 50-year period, and regime persistence, defined as the mean duration of consecutive occurrences. Values are shown for ERA5 as well as for the historical and projected simulations of MPI and EC-Earth3. Projected changes in frequency and persistence are discussed in Sect. 3.2.

In winter, MPI slightly underestimates the NAO+ frequency (26.8%) relative to ERA5 (30%), whereas EC-Earth3 shows closer agreement (29.5%). Both models underestimate persistence (≈5.1 days versus 5.5 days in ERA5). For the Blocking regime, both models underestimate persistence (4.8-5.0 days versus 5.6 days in ERA5) and, to a lesser extent, frequency, particularly in EC-Earth3 (24.8% versus 26.9%). For NAO-, both models overestimate frequency (≈23% versus 19.6% in ERA5), while persistence is underestimated, especially in EC-Earth3. For the Atlantic Ridge regime, both frequency and persistence are well reproduced. Overall, both GCMs reproduce the ranking of regime frequencies found in ERA5 and provide a generally realistic representation of regime persistence, despite some moderate biases in individual regimes.

https://doi.org/10.5194/egusphere-2026-7095
Preprint. Discussion started: 27 November 2026
© Author(s) 2026. CC BY 4.0 License.

In summer, MPI underestimates both frequency and persistence of NAO+ (24.9 % and 4.6 days versus 27.4 % and 5.0 days in ERA5), while EC-Earth3 shows closer agreement. For the Blocking regime, MPI closely matches ERA5 (25.3 % and 5.4 days), while EC-Earth3 underestimates both metrics (22.0 % and 4.5 days). The NAO- regime is well reproduced by both models in terms of frequency and persistence. The Atlantic Ridge regime is slightly overrepresented in both models, with frequencies exceeding ERA5 by approximately 2-3% and persistence by 0.3-0.7 days. Overall, summer weather-regime statistics are reproduced reasonably well by both GCMs. Although the ranking of regime frequencies differs slightly more from ERA5 than in winter, regime frequencies and persistences remain of comparable magnitude to those observed in the reanalysis.

Table 1: Frequency and persistence of weather regimes for winter (NDJFM). For the projections, significance of the change compared to the historic period is given by * if p<0.10 and ** if p<0.05.

Regime	Var	ERA5	MPI hist	MPI SSP2	MPI SSP5	EC-Earth hist	EC-Earth SSP2
NAO+	Freq (%)	30.0	26.8	26.3	26.4	29.5	27.9
	Pers (days)	5.5	5.1	5.1	5.1	5.1	5.2
Blocking	Freq (%)	26.9	25.6	24.6	24.5	24.8	26.2
	Pers (days)	5.6	4.8	5.0	4.8	5.0	4.9
NAO-	Freq (%)	19.6	22.8	23.4	26.8*	23.1	23.0
	Pers (days)	6.0	5.8	5.3	6.8**	5.4	5.6
Atlantic ridge	Freq (%)	23.6	24.8	25.7	22.3	22.5	22.9
	Pers (days)	4.7	4.8	4.9	5.0	4.4	4.6

Table 2: Same as Tab. 1 but for summer (JJA).

Regime	Var	ERA5	MPI hist	MPI SSP2	MPI SSP5	EC-Earth hist	EC-Earth SSP2

https://doi.org/10.5194/egusphere-2026-7095
Preprint. Discussion started: 27 November 2026
© Author(s) 2026. CC BY 4.0 License.

NAO+	Freq (%)	27.4	24.9	28.4	27.5	28.2	27.3
	Pers (days)	5.0	4.6	5.5**	6.0**	5.3	5.3
Blocking	Freq (%)	25.3	25.6	25.5	26.1	22.0	28.3**
	Pers (days)	5.4	5.3	5.2	5.8	4.5	5.5**
NAO-	Freq (%)	24.0	23.6	25.4	23.3	24.4	23.7
	Pers (days)	5.4	5.5	5.5	5.1	5.5	5.3
Atlantic ridge	Freq (%)	23.2	25.9	20.7**	23.1	25.4	20.7**
	Pers (days)	4.3	5.0	4.3*	5.1	4.6	4.3

Figure 3 presents the mean winter precipitation simulated by MAR forced with ERA5, together with precipitation anomalies associated with each weather regime. Mean precipitation is highest at high elevations, reaching approximately 8 mm w.e. day^{-1} in the Swiss Alps, while valley regions typically receive around 3 mm w.e. day^{-1}. Under NAO+ conditions, precipitation is slightly enhanced over the northwestern Alps and reduced elsewhere. In contrast, Blocking is associated with positive anomalies over the southern, primarily Italian, Alps and negative anomalies across most of the remaining Alpine region. NAO- produces widespread positive precipitation anomalies, exceeding 50% in the southern Alps, indicating particularly wet conditions. The Atlantic Ridge regime favors increased precipitation in the northeastern Alps, while drier-than-average conditions prevail elsewhere.

Figure 4 shows the corresponding precipitation patterns for the historical MAR-MPI simulation. Mean precipitation displays a stronger elevation gradient than in MAR-ERA5, with maxima reaching approximately 10 mm w.e. day^{-1} along the Alpine ridge while low-elevation values remain close to 3 mm w.e. day^{-1}. The largest differences relative to MAR-ERA5 occur during NAO+ events, for which precipitation anomalies peak over the southern Alps (up to 70 %) and become negative over the northeastern Alps. This pattern is consistent with the southward displacement of the western circulation compared to ERA5, which shifts the prevailing flow from westerly to southwesterly over the Alps (see Fig. 2).

The Blocking regime exhibits a spatial pattern similar to that of MAR-ERA5, with enhanced precipitation over the southern Alps and reduced precipitation elsewhere, but with substantially larger amplitudes. Negative anomalies reach approximately

https://doi.org/10.5194/egusphere-2026-7095
Preprint. Discussion started: 27 November 2026
© Author(s) 2026. CC BY 4.0 License.

-70 %, compared with values generally between -40 % and -50 % in MAR-ERA5. This amplification is consistent with the closer proximity of the anticyclonic center to the Alps (Fig. 2). In contrast, NAO- events are associated with relatively weak anomalies, generally within +/- 10 %, likely reflecting reduced wind anomalies over the region compared to ERA5. The Atlantic Ridge regime displays a pronounced north-south contrast, broadly similar to MAR-ERA5 but with substantially stronger amplitudes, ranging from approximately -70 % to +70 %, and with a westward extension of the positive anomaly pattern.

Figure 5 presents the historical MAR-EC-Earth3 simulation. Mean winter precipitation is comparable to that simulated by MAR-MPI and remains higher than in MAR-ERA5. For the NAO+ regime, both the spatial structure and magnitude of the precipitation anomalies closely resemble those obtained with MAR-ERA5. A similarly good agreement is found for the Blocking regime, consistent with the close correspondence of the associated circulation patterns shown in Fig. 2.

The NAO- regime also reproduces the ERA5-driven precipitation pattern well, although anomalies are generally stronger and exhibit a more pronounced north-south gradient. Positive anomalies exceed 70 % across large portions of the southern Alps, compared with values closer to 50 % in MAR-ERA5. This difference is consistent with the slightly stronger circulation anomalies simulated by EC-Earth3. Finally, the Atlantic Ridge regime is reproduced well in both pattern and intensity, with the main exception occurring over the northern French Alps, where MAR-EC-Earth3 simulates a mixture of positive and negative anomalies, whereas MAR-ERA5 exhibits weakly negative anomalies of approximately 10-20 %.

https://doi.org/10.5194/egusphere-2026-7095
Preprint. Discussion started: 27 November 2026
© Author(s) 2026. CC BY 4.0 License.

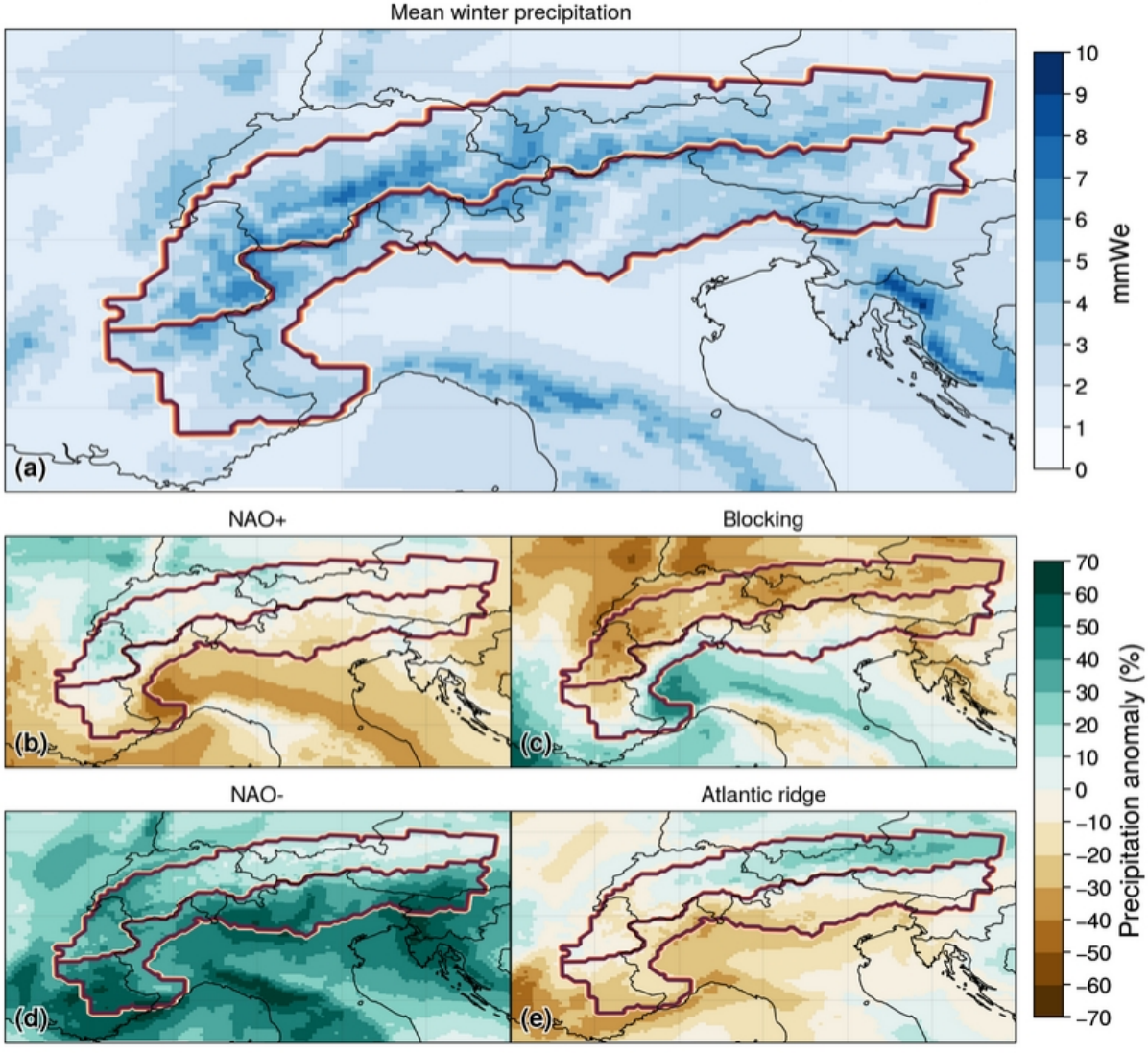
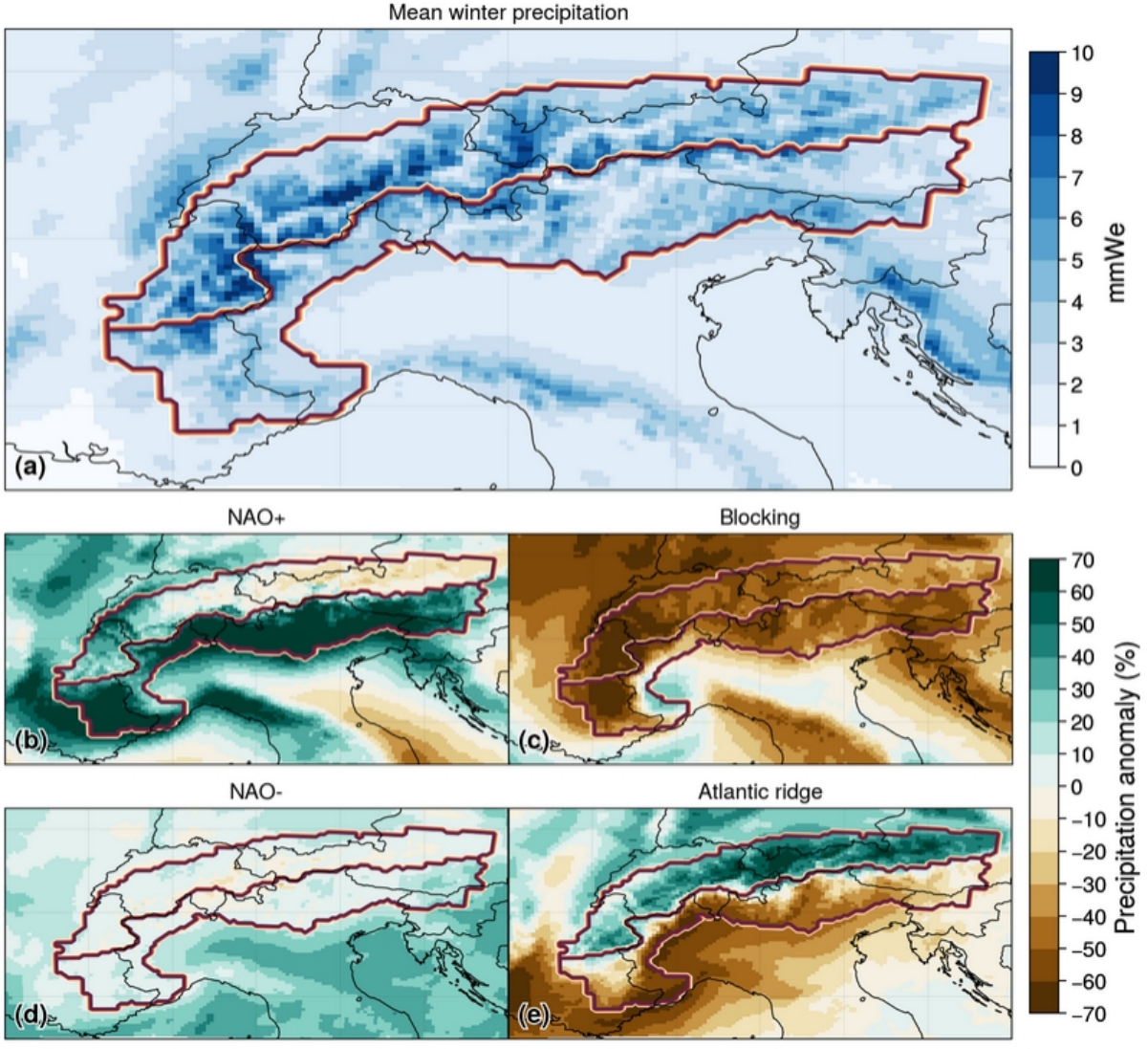


Figure 3: MAR-ERA5 winter precipitation (top) and anomalies by weather regime (bottom) averaged over 1961-2009. The northern and southern boundaries of the Alps as described in Sect. 2.2.2 are superimposed.

https://doi.org/10.5194/egusphere-2026-7095
Preprint. Discussion started: 27 November 2026
© Author(s) 2026. CC BY 4.0 License.



415 **Figure 4: Same as Fig. 3 but for MAR-MPI.**

https://doi.org/10.5194/egusphere-2026-7095
Preprint. Discussion started: 27 November 2026
© Author(s) 2026. CC BY 4.0 License.

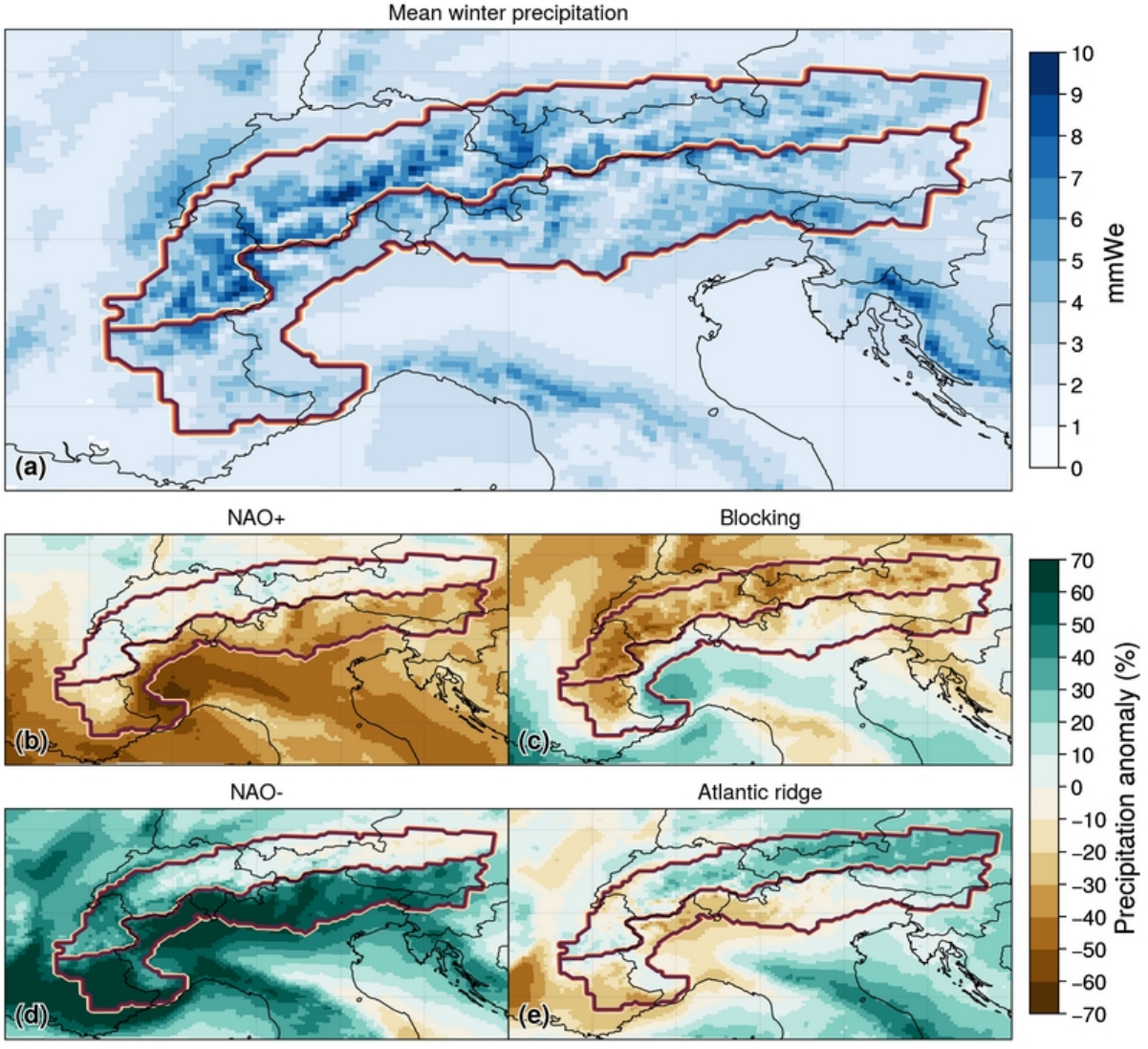


Figure 5: Same as Fig. 3 but for MAR-EC-Earth3.

These climatological means of precipitation are summarised in Fig. 6, which reports mean winter precipitation and relative anomalies (in %) for all three simulations over the northern and southern Alps. The color shading follows the same scale as in Figs. 3-5. The table confirms that EC-Earth3 reproduces a winter climatology that is closer to ERA5, a consistency that is preserved in the downscaled MAR simulation. In contrast, MAR-MPI exhibits larger deviations, particularly for the NAO+ regime, where discrepancies in both magnitude and spatial structure are most pronounced.

Figure 7 presents the corresponding results for summer during the historical period. The associated maps are provided in Appendix B (Figs. B1-B4), which constitute the summer counterpart to Figs. 2-5. In contrast to winter, both GCM-driven simulations produce lower mean seasonal precipitation than the ERA5-driven simulation. This reversal of the winter behaviour suggests a marked seasonal dependence in the response of MAR to the driving data.

https://doi.org/10.5194/egusphere-2026-7095
Preprint. Discussion started: 27 November 2026
© Author(s) 2026. CC BY 4.0 License.

Compared with winter, precipitation anomalies associated with weather regimes are generally weaker. In MAR-ERA5, summer anomalies typically range between -10% and +10%, whereas winter anomalies reach approximately -30% to +40%. The GCM-driven simulations also exhibit weaker summer anomalies than winter anomalies, although their amplitude remains larger than in MAR-ERA5, reaching approximately -30% to +20%.

For the NAO+ regime, MAR-MPI reproduces the spatial pattern of the ERA5-driven simulation but substantially overestimates the anomaly magnitude, by approximately a factor of two in the northern Alps and three in the southern Alps. MAR-EC-Earth3 captures both the sign and magnitude of the anomaly in the southern Alps, but simulates near-neutral conditions in the north. Under Blocking conditions, MAR-MPI produces weak positive anomalies (~5%), in close agreement with MAR-ERA5, whereas MAR-EC-Earth3 overestimates the response in both regions, with anomalies of approximately 20%.

The NAO- regime is generally well represented by both GCM-driven simulations. MAR-ERA5 exhibits weak positive anomalies in both regions, and the GCM-driven simulations reproduce this overall signal. However, MAR-MPI overestimates the anomaly in the southern Alps (10.2% compared with 3.8% in MAR-ERA5), while both GCM-driven simulations underestimate the anomaly in the north. For the Atlantic Ridge regime, MAR-ERA5 shows a weak positive anomaly in the northern Alps and near-neutral conditions in the south. MAR-MPI reproduces the sign of the northern anomaly but approximately doubles its amplitude and simulates a moderate positive anomaly in the south. In contrast, MAR-EC-Earth3 produces pronounced negative anomalies, reaching -21.9% in the northern Alps, and therefore departs substantially from the ERA5-driven simulation.

Overall, the MPI-driven simulations reproduce the summer precipitation climatology and regime-dependent anomalies more faithfully than MAR-EC-Earth3, in contrast to winter, when MAR-EC-Earth3 generally exhibits better agreement with MAR-ERA5. Two additional features emerge from this comparison: (i) the GCM-driven simulations produce systematically stronger regime-dependent anomalies than MAR-ERA5, and (ii) they yield lower mean seasonal precipitation than MAR-ERA5, whereas the opposite is found in winter. These differences may reflect biases inherited from the driving GCMs, differences arising from the downscaling of coarser-resolution boundary conditions (~100 km) compared with ERA5 (~31 km), or a combination of both factors. Investigating the origin of these behaviours lies beyond the scope of the present study.

Model	Region	Mean	NAO+	Blocking	NAO-	Atlantic ridge
ERA5	North	3.85	2.9	-27.6	20.7	10.3
	South	3.45	-11.7	-6.5	42.4	-12.3
MPI	North	4.72	9.5	-48.2	3.3	36.9
	South	3.67	60.5	-43.4	7.0	-27.5
EC-Earth3	North	4.37	-2.7	-29.2	17.1	18.6
	South	3.55	-30.9	-9.9	56.0	-4.2

Figure 6: Winter climatology, 1961-2009. Mean values are in mmWe. Weather regime values are precipitation anomalies relative to the mean, in percent.

https://doi.org/10.5194/egusphere-2026-7095
Preprint. Discussion started: 27 November 2026
© Author(s) 2026. CC BY 4.0 License.

Model	Region	Mean	NAO+	Blocking	NAO-	Atlantic ridge
ERA5	North	4.91	-9.9	-2.7	8.1	6.3
	South	4.03	-10.9	7.4	3.8	0.7
MPI	North	2.92	-19.2	4.2	1.3	13.1
	South	2.02	-28.2	3.8	10.2	14.0
EC-Earth3	North	3.24	0.6	19.6	3.6	-21.9
	South	2.68	-7.5	19.0	4.3	-12.8

Figure 7: Same as Fig. 6 but for summer.

3.2 Projected changes

In this section, the large-scale circulation and the associated precipitation patterns in the Alps in the projected period (2050-2099) are compared to those simulated in the historic period (1961-2009) in order to quantify the trends simulated by the GCMs modulated by the local effect of MAR. The projections are made with MPI-ESM1-2-HR for two scenarios - SSP2-4.5 and SSP5-8.5 - and with EC-Earth3 for the SSP2-4.5 scenario.

https://doi.org/10.5194/egusphere-2026-7095
Preprint. Discussion started: 27 November 2026
© Author(s) 2026. CC BY 4.0 License.

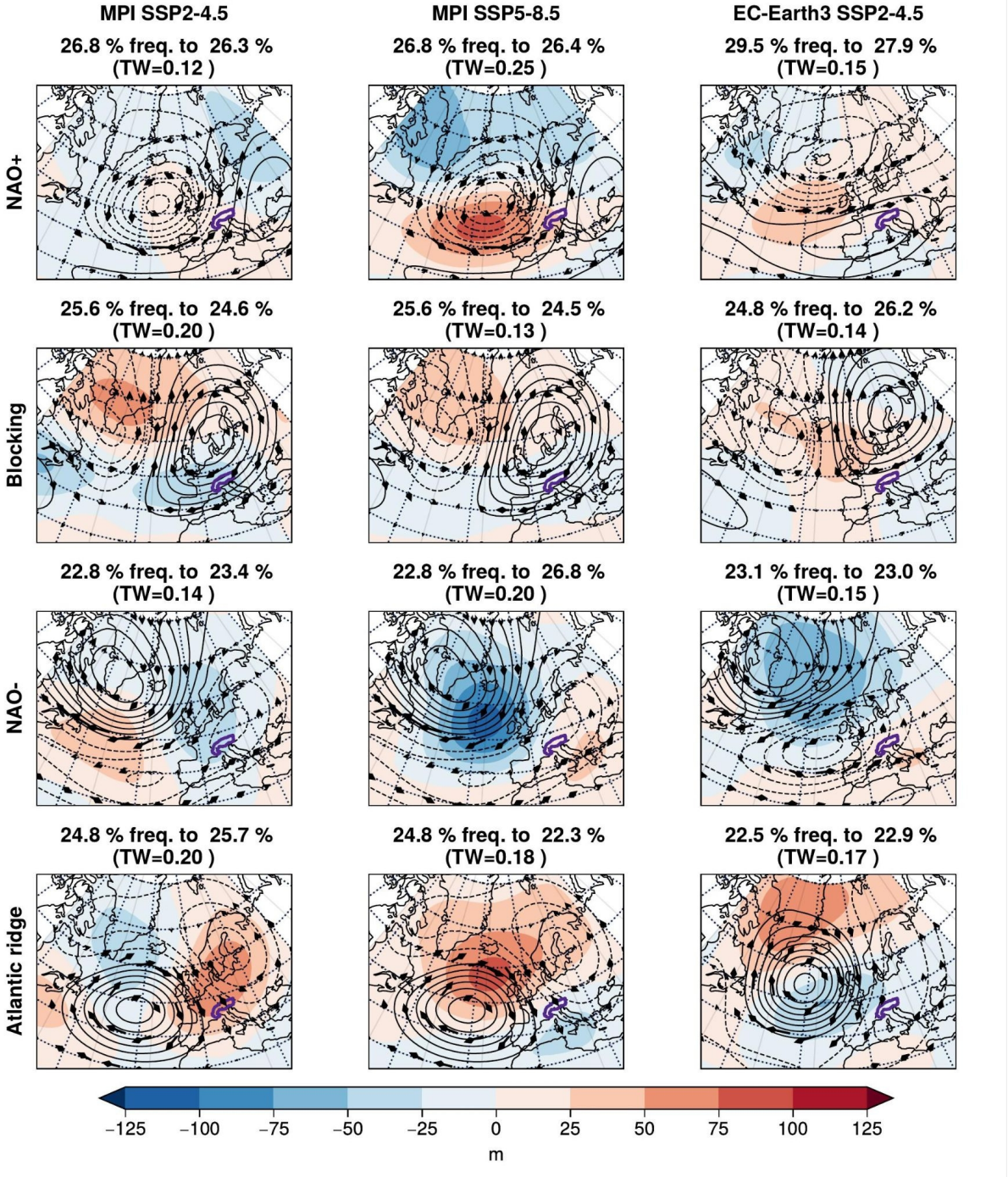


Figure 8: Difference in winter (NDJFM) geopotential height between projection and historical period (shading). Geopotential height and wind climatology for the historical period are shown with isolines and arrows respectively. Solid lines indicate positive values and dashed lines indicate negative values, with a contour interval of 25 m.

https://doi.org/10.5194/egusphere-2026-7095
Preprint. Discussion started: 27 November 2026
© Author(s) 2026. CC BY 4.0 License.

Figure 8 illustrates the projected changes in large-scale circulation across the three simulations. Differences in Z500 anomalies between the projected and historical periods are shown in color, while historical climatology is indicated with contours (with arrows representing the wind anomalies). The frequency of occurrence of each weather regime is provided for both periods, together with the Teweles-Wobus score (TW), which quantifies the similarity between projected and historical patterns (see Sect. 2.2.3). Unlike a Euclidean distance, the TW score emphasizes structural differences independent of intensity and ranges from 0 (identical patterns) to 1 (opposite patterns). Lower values therefore indicate greater stability of the regime between periods.

For NAO+, only minor changes are simulated in MPI SSP2-4.5. In contrast, MPI SSP5-8.5 exhibits a clear northwestward displacement of both the low and high pressure systems. In EC-Earth3, the structural change is lower and exhibits a westward shift with a weakening on the southern flank. For the Blocking regime, MPI simulations suggest a reorganization of the circulation pattern, characterized by positive changes over the northern part of the regime and negative changes over its southern part, whereas EC-Earth3 projects a southwestward shift of the anticyclonic center. For NAO-, MPI SSP2-4.5 indicates a southward displacement of the high pressure system, while SSP5-8.5 projects a northwestward shift. EC-Earth3 instead shows a weakening on the anticyclone's eastern flank, and therefore predominantly westward displacement. Finally, for the Atlantic Ridge regime, MPI SSP2-4.5 suggests a slight counterclockwise torsion of the ridge, whereas both MPI SSP5-8.5 and EC-Earth3 project a northward shift of the ridge.

The largest structural change is found for NAO+ in MPI SSP5-8.5 (TW = 0.25), while the smallest occurs for NAO+ in MPI SSP2-4.5 (TW = 0.12). The contrast between these two simulations illustrates the substantial variability that can affect weather-regime structure. It may reflect differences in the forced response, internal climate variability, or a combination of both. Given the limited ensemble size considered here, these contributions cannot be disentangled. As for EC-Earth3, the simulation exhibits weak structural change across the board, with a TW score between 0.14 and 0.17.

The projected evolution of regime frequency and persistence is summarized in Tabs. 1 and 2. Building on the historical evaluation presented in Sect. 3.1, we now examine whether significant changes emerge in the future simulations.

In winter, projected changes for the NAO+ regime are generally small and not statistically significant. For the Blocking regime, no significant changes are projected either. For the NAO- regime, a significant increase in both frequency (from 22.8 to 26.8 %, $p < 0.10$) and persistence (from 5.8 to 6.8 days, $p < 0.05$) is simulated in MPI SSP5-8.5 relative to its historical counterpart, whereas no significant changes are found for SSP2-4.5. For the Atlantic Ridge regime, MPI simulations suggest opposite (but non-significant) tendencies depending on the scenario. Overall, projected changes in winter weather-regime frequency and persistence remain limited, with the only significant signal being an increase in the occurrence and persistence of NAO- in MPI SSP5-8.5.

In summer, for the NAO+ regime, projections remain stable in EC-Earth3, whereas MPI simulates a non-significant increase in frequency and a significant increase in persistence (from 4.6 to 5.5-6.0 days, $p < 0.05$). For the Blocking regime, MPI shows little change, whereas EC-Earth3 exhibits a significant increase in both frequency (from 22.0 to 28.3 %, $p < 0.05$) and persistence (from 4.5 to 5.5 days, $p < 0.05$). The NAO- regime remains largely unchanged in future projections. For the Atlantic Ridge regime under SSP2-4.5, both models simulate a significant decrease in frequency (to 20.7%, $p < 0.05$) and a reduction in persistence (to 4.3 days, significant in MPI only). No significant change is found for MPI SSP5-8.5. Overall, summer exhibits more significant changes in regime behaviour than winter, but no systematic response emerges across all models and weather regimes.

https://doi.org/10.5194/egusphere-2026-7095
Preprint. Discussion started: 27 November 2026
© Author(s) 2026. CC BY 4.0 License.

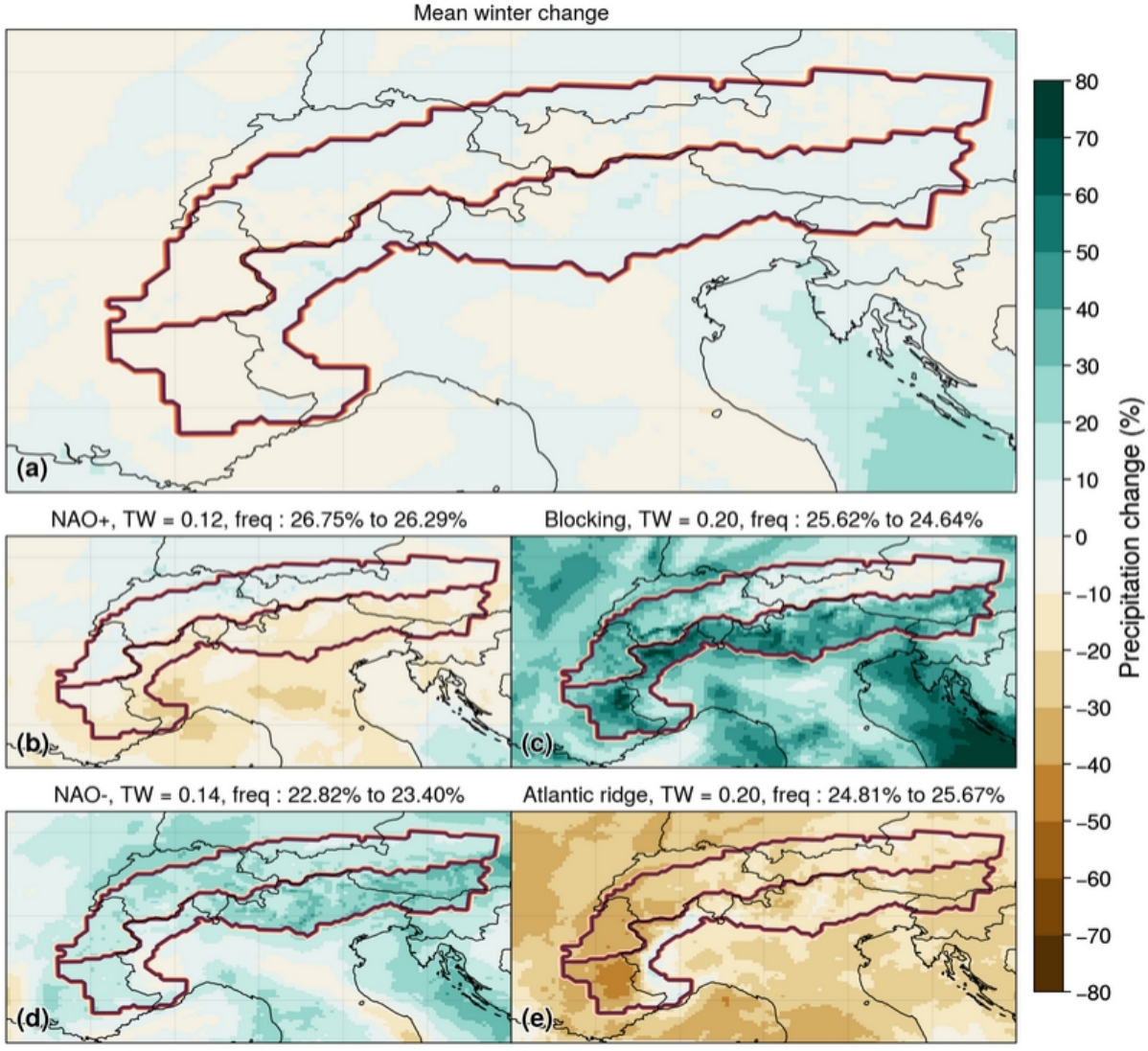


Figure 9: MAR-MPI winter (NDJFM) precipitation changes between projection (SSP2-4.5, 2050-2099) and historic period (1961-2009), by weather regime. The Teweles-Wobus score between the two periods for each weather regime is given, as well as the frequency changes for each weather regime.

Figure 9 shows the relative change in winter precipitation over the Alps between 1961-2009 and 2050-2099 for the MAR-MPI SSP2-4.5 simulation, both for the seasonal mean (Fig. 9a) and for individual weather regimes (Figs. 9b-e).

At the seasonal scale, changes remain modest (generally below 10 %) and exhibit no clear spatial structure. In contrast, regime-specific responses reveal more distinct patterns. For NAO+, changes are relatively weak (around 10-20 %) but display a north-south contrast, with a slight increase in precipitation over the northern Alps and a decrease over the southern Alps. Under Blocking conditions, precipitation increases across most of the region, with a stronger signal (generally above 40 %) in the southern Alps. This is consistent with the northward and westward displacement of the anticyclone (Fig. 8), which places the Alps more directly under easterly flow.

https://doi.org/10.5194/egusphere-2026-7095
Preprint. Discussion started: 27 November 2026
© Author(s) 2026. CC BY 4.0 License.

For NAO-, precipitation also increases, although less markedly than for the Blocking regime. The southward shift of the cyclonic center of action (Fig. 8) enhances southwesterly flow towards the Alps, favoring increased precipitation. In contrast, the Atlantic Ridge regime is associated with a general decrease in precipitation, around 20 % and up to 50 %, which can be linked to the displacement of the circulation pattern which shifts the strongest flow away from the Alps.

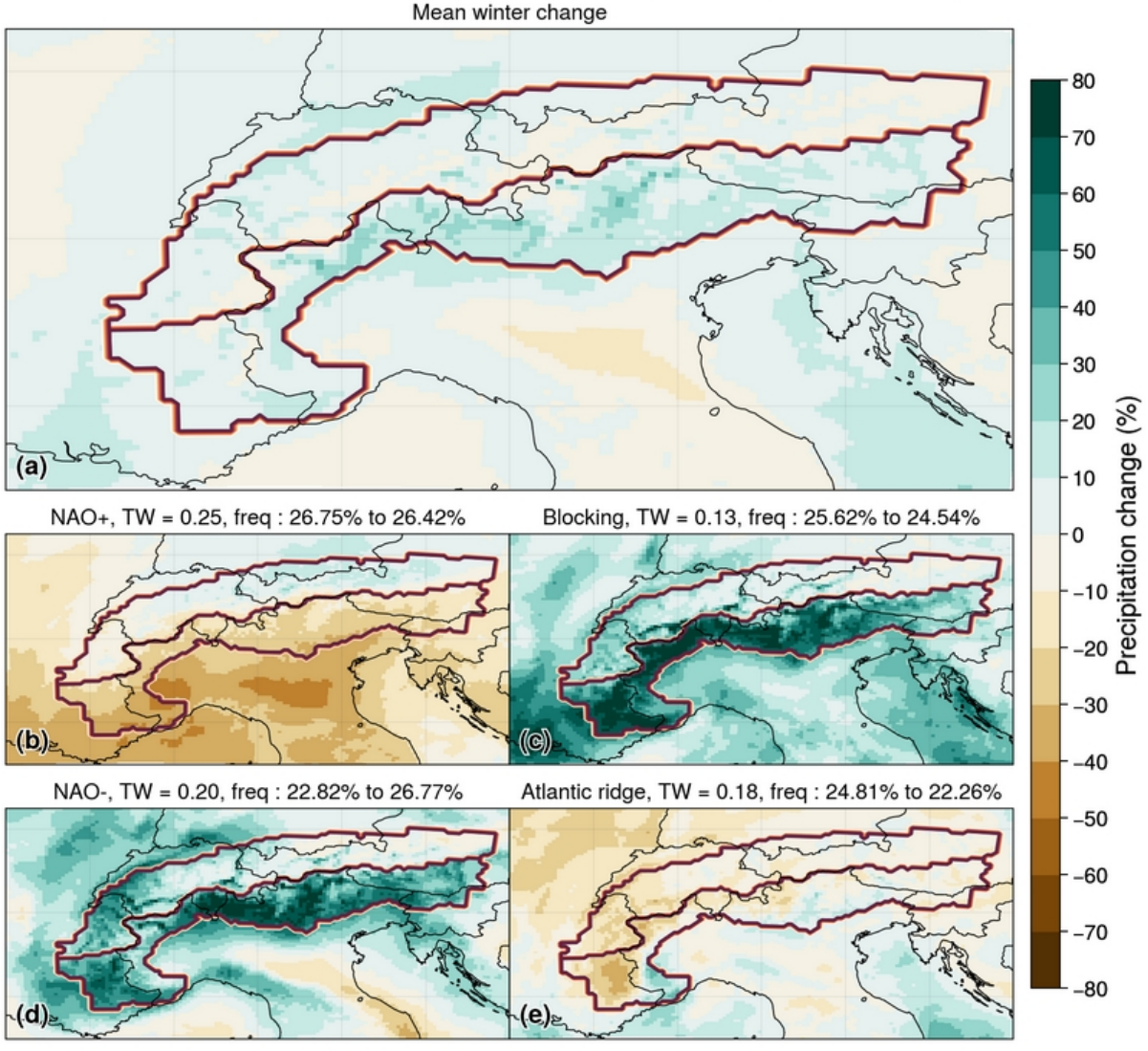


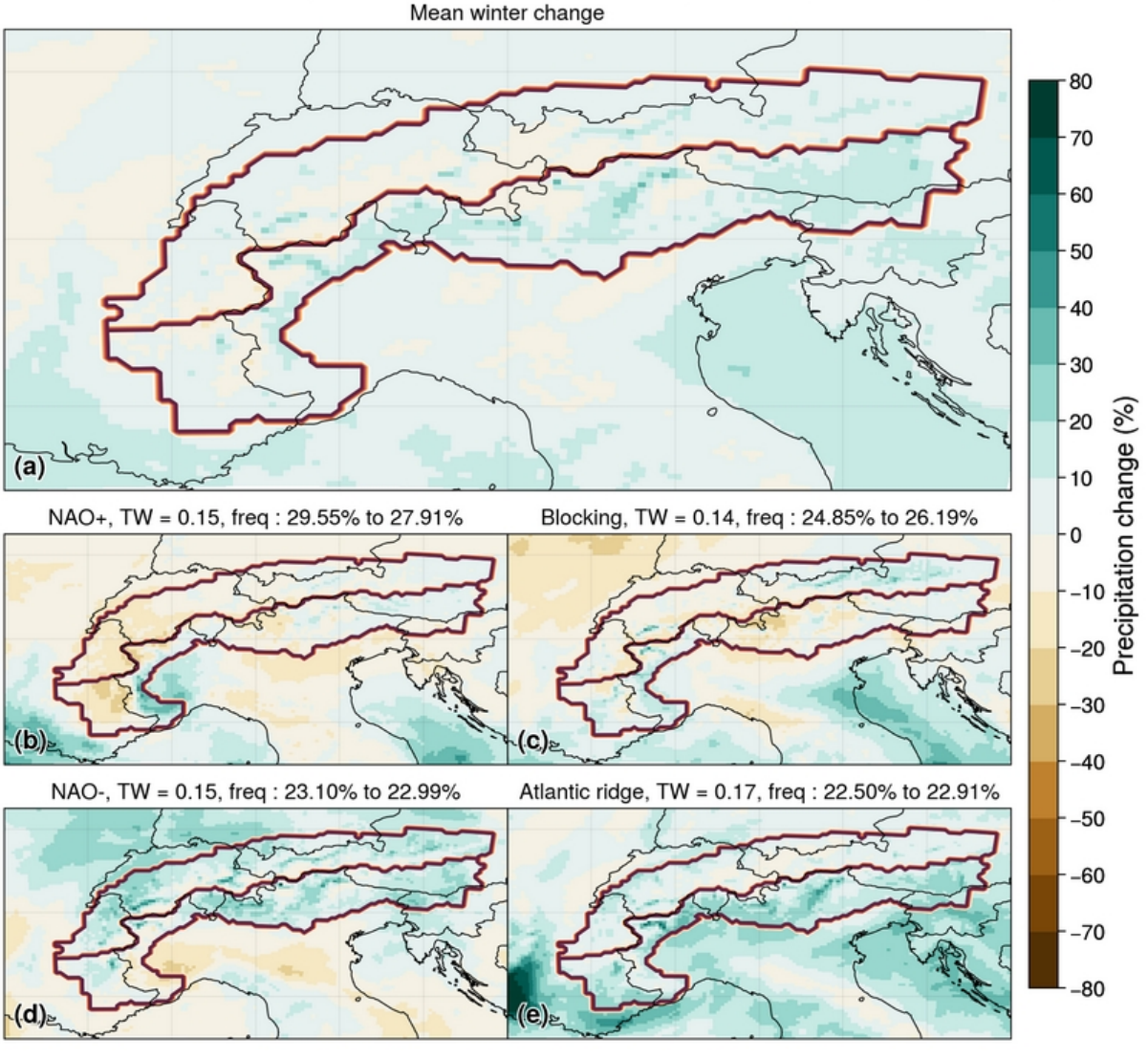
Figure 10: MAR-MPI winter precipitation changes between projection (SSP5-8.5, 2050-2099) and historical period (1961-2009), by weather regime. The Teweles-Wobus score between the two periods for each weather regime is given, as well as the frequency changes for each weather regime.

Figure 10 presents the corresponding changes for the SSP5-8.5 scenario using the same model. In this case, a more pronounced increase in precipitation is simulated, particularly over the southern Alps, where values reach up to 30-40%. For NAO+, precipitation decreases in the southern Alps while exhibiting spatially heterogeneous changes in the north. This behavior is consistent with the low pressure system shifting northwestward, away from the Alpine region (Fig. 8).

https://doi.org/10.5194/egusphere-2026-7095
Preprint. Discussion started: 27 November 2026
© Author(s) 2026. CC BY 4.0 License.

The Blocking regime shows a substantial increase in precipitation, especially in the southern Alps, with local values approaching 80%. This response is qualitatively similar to that found under SSP2-4.5 but with greater magnitude, likely reflecting enhanced atmospheric moisture availability in a warmer climate. A comparable pattern is simulated for NAO-, again consistent with the northwestward displacement of the cyclonic center, which increases moisture advection toward the Alps. For the Atlantic Ridge regime, precipitation generally decreases, although localized increases are also present. This more heterogeneous signal may reflect a circulation shift (Fig. 8) that only partially displaces the main flow away from the Alps, in contrast to SSP2-4.5.

Overall, the spatial structure of the signal is similar to that of MAR-MPI under the SSP2-4.5 scenario, except with larger magnitudes.



https://doi.org/10.5194/egusphere-2026-7095
Preprint. Discussion started: 27 November 2026
© Author(s) 2026. CC BY 4.0 License.

Figure 11: MAR-EC-Earth3 winter precipitation changes between projection (SSP2-4.5, 2050-2099) and historical period (1961-2009), by weather regime. The Teweles-Wobus score between the two periods for each weather regime is given, as well as the frequency changes for each weather regime.

Figure 11 shows the same diagnostics for MAR-EC-Earth3. The seasonal mean indicates a slight decrease in precipitation at higher elevations and a modest increase at lower elevations. For NAO+, spatial patterns are more heterogeneous, with positive trends over the Italian and Austrian Alps and negative trends over the Swiss and French Alps. This east-west contrast is consistent with the westward displacement of the anticyclone (Fig. 8), which enhances moisture transport toward the eastern Alps.

Under Blocking conditions, a similarly heterogeneous pattern is observed. While part of this structure may be linked to circulation changes, internal variability likely contributes to the noisier signal. The NAO- regime exhibits a more spatially coherent increase in precipitation, although with smaller amplitudes than in MPI. Finally, the Atlantic Ridge regime shows predominantly positive trends (generally between 10 and 30 %), particularly over the southern Alps, consistent with a displacement of the anticyclone that favors moisture advection toward the region.

Overall, regime-specific changes are more pronounced and spatially structured than seasonal-mean changes. This contrast is particularly evident in MPI, which exhibits strong and coherent signals, whereas EC-Earth3 displays weaker and more spatially variable responses. Only the NAO- regime exhibits a relatively consistent increase in precipitation across all three experiments and all of the Alps.

Model	Region	Mean	NAO+	Blocking	NAO-	Atlantic ridge
MPI SSP2-4.5	North	-0.2	1.1	18.1**	17.4**	-21.9**
	South	0.7	-11.7**	39.0**	19.7**	-21.0**
MPI SSP5-8.5	North	3.1	-0.0	14.7**	16.6**	-8.4**
	South	9.2**	-23.6**	50.3**	44.8**	-6.2**
EC-Earth3 SSP2-4.5	North	2.5	-5.2*	-0.1	10.7**	4.8
	South	6.1	-2.2	-1.4	8.5*	15.5**

Figure 12: Winter changes in precipitation. Both mean and weather regime values are relative changes between 1961-2009 and 2050-2099, in percent. The significance of the change compared to the historic period is given by an asterisk (*) if p<0.10 and ** if p<0.05 (see Sect. 2.2.4).

Model	Region	Mean	NAO+	Blocking	NAO-	Atlantic ridge
MPI SSP2-4.5	North	-10.3**	-4.3	10.0*	-26.6**	-13.6**
	South	-12.8**	4.9	5.6	-37.1**	-11.9**
MPI SSP5-8.5	North	-16.3**	-1.9	-12.3**	-21.7**	-22.9**
	South	-13.4**	2.5	-10.8**	-20.8**	-13.6**
EC-Earth3 SSP2-4.5	North	0.1	2.7	-2.5	-10.3**	5.9
	South	6.7**	11.5**	3.7	-6.9*	19.8**

Figure 13: Same as Fig. 12 but for summer.

https://doi.org/10.5194/egusphere-2026-7095
Preprint. Discussion started: 27 November 2026
© Author(s) 2026. CC BY 4.0 License.

The results shown in Figures 9-11 are synthesized in Fig. 12, where values are spatially averaged over the northern and southern Alps.

Changes in mean winter precipitation are generally not statistically significant, with the notable exception of a significant increase of 9.2% in the southern Alps for MAR-MPI SSP5-8.5. In contrast, regime-specific changes are more frequently significant, particularly in the MAR-MPI simulations, consistent with the patterns described in Figures 9-11. Indeed, nearly all regime-specific changes are significant in the MAR-MPI simulations, with the exception of NAO+ in the northern Alps.

A notable feature of the MAR-MPI experiments is that the substantial increases in precipitation associated with the Blocking and NAO- regimes, especially in the southern Alps, are partially offset by significant decreases during NAO+ and Atlantic Ridge conditions. As a result, changes in seasonal-mean precipitation remain comparatively weak despite pronounced regime-specific responses. A similar, although less marked, compensation is observed in the northern Alps.

Figure 13 summarizes the corresponding results for summer (see Appendix C for the spatial maps). In contrast to winter, seasonal mean changes are more robust. The MAR-MPI simulations project a generalized and statistically significant decrease in precipitation of approximately 10-15 %, whereas MAR-EC-Earth3 indicates a modest but significant increase (+6.7%) in the southern Alps. All simulations consistently project a decrease in precipitation associated with the NAO- regime, which is significant in most cases and particularly pronounced in MAR-MPI SSP2-4.5, where reductions approach 40% in the southern Alps. For the other regimes, responses are more heterogeneous. Under Atlantic Ridge conditions, both MAR-MPI simulations exhibit significant decreases in precipitation (approximately 10-20 %), whereas MAR-EC-Earth3 projects an increase that reaches nearly 20% in the southern Alps and is statistically significant. For the Blocking regime, the two MPI scenarios disagree on the sign of the response: SSP2-4.5 indicates a weak increase, while SSP5-8.5 projects a significant decrease of 10-12 %. MAR-EC-Earth3 exhibits comparatively weak and spatially heterogeneous changes. Finally, NAO+ is characterized by generally weak and contrasting responses across simulations, except for a significant increase in the southern Alps in MAR-EC-Earth3 (+11.5%).

Overall, NAO- emerges as the regime exhibiting the most coherent response across models and seasons, with increased precipitation in winter and decreased precipitation in summer. Atlantic Ridge also displays a consistent model-dependent response, with precipitation decreases in the MPI-driven simulations and increases in MAR-EC-Earth3. In contrast, the Blocking regime exhibits substantial changes in MAR-MPI but little response in MAR-EC-Earth3, while the sign of the summer response varies between MPI scenarios. NAO+ shows the weakest and least consistent signals, suggesting a comparatively limited sensitivity to the projected circulation changes considered here.

4 Discussion and conclusion

The present study investigated the links between large-scale circulation and Alpine precipitation by combining weather-regime analysis of two CMIP6 GCMs (MPI-ESM1-2-HR and EC-Earth3) with some of their experiments dynamically downscaled over the Alps with the regional model MAR. Weather regimes were identified using the WTD methodology based on PCA dimensionality reduction followed by k-means clustering with four clusters, both in winter (NDJFM) and summer (JJA).

https://doi.org/10.5194/egusphere-2026-7095
Preprint. Discussion started: 27 November 2026
© Author(s) 2026. CC BY 4.0 License.

Overall, both GCMs reproduce the canonical winter North Atlantic-European weather regimes with sufficient fidelity to allow a one-to-one comparison with ERA5. Some discrepancies are nevertheless apparent, particularly for the NAO+ regime in MPI, whose circulation pattern resembles an Atlantic Low configuration more closely than the canonical NAO+ pattern. This result is consistent with Harvey et al. (2020), who reported a southward bias of the North Atlantic jet in CMIP6 models. However, differences between ERA5 and the GCMs should not necessarily be interpreted as model deficiencies. The analysis of ten MPI realizations presented in Appendix A highlights the substantial role of internal climate variability in weather-regime structures. Because GCM simulations represent independent realizations of the climate system, exact agreement with a reanalysis cannot be expected even in the absence of model biases. Similar conclusions apply to summer, although weather regimes are generally less distinct than in winter, consistent with previous studies (e.g. Cortesi et al., 2021).

The historical simulations indicate that both GCMs reproduce weather-regime patterns, frequencies, and persistence reasonably well. A seasonal contrast nevertheless emerges, with EC-Earth3 showing closer agreement with ERA5 in winter and MPI performing slightly better in summer. This behaviour is reflected in the downscaled MAR simulations, where regime-specific precipitation anomalies generally resemble those obtained with MAR-ERA5 more closely for EC-Earth3 in winter and for MPI in summer. Two additional features emerge from the historical precipitation climatologies. First, the GCM-driven MAR simulations produce higher winter precipitation than MAR-ERA5, particularly at high elevations, whereas summer precipitation is generally lower. Second, precipitation anomalies associated with individual weather regimes tend to be amplified in the GCM-driven simulations, especially during winter. These differences may arise from biases in the driving GCMs, differences in the downscaling of coarse-resolution GCM fields compared with ERA5, or differences between MAR versions. Further work would be required to disentangle the relative importance of these factors.

Projected changes in weather-regime structure, frequency, and persistence are heterogeneous and lack a consistent response across simulations. Winter circulation changes remain limited overall, although some regimes exhibit noticeable structural modifications, particularly in MPI SSP5-8.5. Summer changes are generally larger, which may reflect the weaker regime character of summer circulation and the greater role of local convective processes (Beck et al., 2007; Cortesi et al., 2019). The most notable circulation change identified here is the increase in frequency and persistence of the NAO- regime in MPI SSP5-8.5. Previous studies have suggested that Arctic sea-ice decline, Arctic amplification, and stratospheric changes may favour NAO- conditions (Jaiser et al., 2012; Fabiano et al., 2021), although these mechanisms remain highly debated and are not consistently reproduced across models (Rousi et al., 2021). Given the limited number of simulations considered here, it is not possible to determine whether the simulated NAO- increase reflects a forced response, internal variability, or a combination of both.

More broadly, the projected weather-regime changes remain highly uncertain. Fabiano et al. (2021) showed that future weather-regime responses are characterized by substantial inter-model spread and are influenced by multiple competing drivers, particularly for NAO-related regimes. Likewise, Rivosecchi et al. (2024) found that internal variability dominates over externally forced NAO changes in future precipitation projections. These results are consistent with the variability evident among MPI realizations (Appendix A) and suggest that distinguishing forced weather-regime changes from internal variability remains a major challenge when interpreting weather-regime responses from a small ensemble of simulations. This also has implications for the selection of driving GCMs in regional climate studies. The variability among MPI realizations shown in Appendix A indicates that, over the North Atlantic-European sector, differences in large-scale circulation associated with internal variability can be of similar magnitude to differences between individual GCMs.

https://doi.org/10.5194/egusphere-2026-7095
Preprint. Discussion started: 27 November 2026
© Author(s) 2026. CC BY 4.0 License.

Consequently, assessing a model solely on the basis of a single realization may lead to an over-interpretation of model-specific biases. Whenever computationally feasible, ensembles of realizations should therefore be considered alongside multi-model ensembles to better characterize the uncertainty associated with future circulation and precipitation changes.

The precipitation response exhibits a markedly different behaviour from the weather-regime response itself. In winter, seasonal-mean precipitation changes generally remain modest (<10 %), whereas regime-conditioned changes are often large and statistically significant. In the MPI-driven simulations, substantial increases in precipitation associated with Blocking and NAO- are largely compensated by decreases associated with NAO+ and Atlantic Ridge conditions, resulting in weak seasonal-mean signals. A similar, although less pronounced, compensation effect is also evident in EC-Earth3. This result highlights the limitations of analyses based solely on seasonal means and demonstrates the added value of a weather-regime framework for investigating precipitation changes at middle latitudes and particularly in complex mountain regions. By conditioning precipitation on large-scale circulation states, it becomes possible to identify responses that would otherwise remain hidden in seasonal aggregates. This finding is consistent with previous work showing that atmospheric circulation strongly modulates Alpine precipitation and precipitation extremes (Blanchet et al., 2021a), and more broadly with recent evidence that recurrent weather patterns and jet-stream variability exert a major control on European hydroclimate variability and extremes across a wide range of timescales (Brönnimann et al., 2025).

Summer exhibits a different behaviour than winter. In the MPI simulations, significant decreases in seasonal precipitation emerge, primarily driven by reductions in precipitation associated with the NAO- and the Atlantic Ridge regimes. EC-Earth3 produces a more heterogeneous response, although the decrease in NAO- precipitation is again present, making it the most consistent precipitation signal across simulations. Interestingly, substantial precipitation changes often occur despite relatively modest changes in weather-regime characteristics. This suggests that circulation changes alone are insufficient to explain the projected precipitation signals. At the same time, the absence of a consistent response across models and scenarios indicates that thermodynamic effects cannot be isolated from circulation influences in the present framework. This interpretation is consistent with Rivosecchi et al. (2024), who found that the NAO explains a decreasing fraction of future precipitation-extreme variability despite remaining an important circulation driver.

The present results therefore support the view that future Alpine precipitation changes arise from a complex interplay between dynamical and thermodynamical processes. De Vries et al. (2022) showed that, during the summer, the location of precipitation transition zones depends strongly on whether circulation and thermodynamic effects are considered together or separately. Similarly, the results presented here suggest that changes in weather-regime characteristics and changes in atmospheric moisture availability are likely intertwined. However, the limited ensemble size does not permit a quantitative attribution of their respective contributions. Future work could address this limitation using circulation-analogue approaches similar to those employed by de Vries et al. (2022), which make it possible to estimate the relative contributions of circulation changes and thermodynamic changes by comparing future climate states with historical analogues exhibiting similar large-scale circulation patterns.

The use of the regional model MAR at a relatively fine resolution (7km), able to describe the main topographic features, is motivated by the strong influence of topography on Alpine precipitation. At the horizontal resolution of contemporary GCMs, the Alpine chain is heavily smoothed, limiting the representation of orographic uplift and associated precipitation gradients. Dynamical downscaling partly alleviates this limitation by providing a more realistic representation of topography and mesoscale atmospheric processes. Previous studies have shown that regional climate models provide substantial added

https://doi.org/10.5194/egusphere-2026-7095
Preprint. Discussion started: 27 November 2026
© Author(s) 2026. CC BY 4.0 License.

value for precipitation over mountainous regions, particularly in the Alps, where the representation of precipitation patterns and extremes benefits from increased resolution (Torma et al., 2015; Rummukainen, 2015). This added value comes at a substantial computational cost. Running MAR at 7 km resolution over multi-decadal periods restricts not only the number of GCMs that can be considered, but also the number of realizations available for each model. Given the important role of internal variability highlighted in this study, particularly for weather-regime characteristics, this limitation may be as important as the restriction on the number of GCMs themselves. The present study should therefore be viewed primarily as an investigation of circulation-precipitation relationships and their potential evolution under climate change, rather than as a comprehensive assessment of projection uncertainty.

The results further emphasize the importance of accurately representing large-scale circulation when assessing future Alpine precipitation. Although both EC-Earth3 and MPI reproduce the canonical North Atlantic-European weather regimes with reasonable fidelity, the remaining circulation biases are reflected in the downscaled precipitation patterns. This finding is consistent with Cusinato et al. (2021), who showed that CMIP6 models generally provide a realistic representation of major modes of atmospheric variability and suggested that their influence on European precipitation may strengthen under strong greenhouse-gas forcing. At the same time, Halifa-Marín et al. (2025) argued that residual deficiencies in the simulation of the NAO remain a significant source of uncertainty in future European precipitation projections. Together, these studies support the relevance of weather-regime approaches for investigating Alpine precipitation change.

Finally, future research could extend the present framework beyond mean weather-regime characteristics to investigate changes in regime variability, predictability, and extremes. Bracegirdle (2022) suggested that CMIP6 models underestimate NAO variability, whereas Fuentes-Franco et al. (2023) reported a future reduction in NAO variability associated with changes in extreme winter precipitation over northern Europe. Combined with the findings of Rivosecchi et al. (2024), these studies suggest that the relationship between circulation variability and precipitation may itself evolve under climate change. Investigating variability and extremes within individual weather regimes as suggested in our study therefore appears to be a promising avenue for improving our understanding of future Alpine hydroclimate change.

Appendices

A – Internal variability of weather regimes in MPI-ESM1-2-HR

This appendix illustrates the role of internal variability in the representation of weather regimes in MPI-ESM1-2-HR.

Figure A1 shows the four weather regimes identified in ten different realizations of MPI-ESM1-2-HR, together with ERA5 as a reference. Realization r1 corresponds to the simulation used throughout the main text. Weather regimes were identified using the methodology described in Sect. 2.2.1, and the resulting clusters were assigned to the canonical North Atlantic-European weather regimes through visual inspection.

It should first be noted that this assignment is not always unambiguous. In realizations r4, r6, and r10, the regime identified as Atlantic Ridge exhibits characteristics closer to a NAO+ regime, while the corresponding NAO+ regime resembles an Atlantic Low configuration. Nevertheless, for consistency with the main analysis and to preserve a one-to-one correspondence between realizations, the same classification is retained throughout this appendix.

https://doi.org/10.5194/egusphere-2026-7095
Preprint. Discussion started: 27 November 2026
© Author(s) 2026. CC BY 4.0 License.

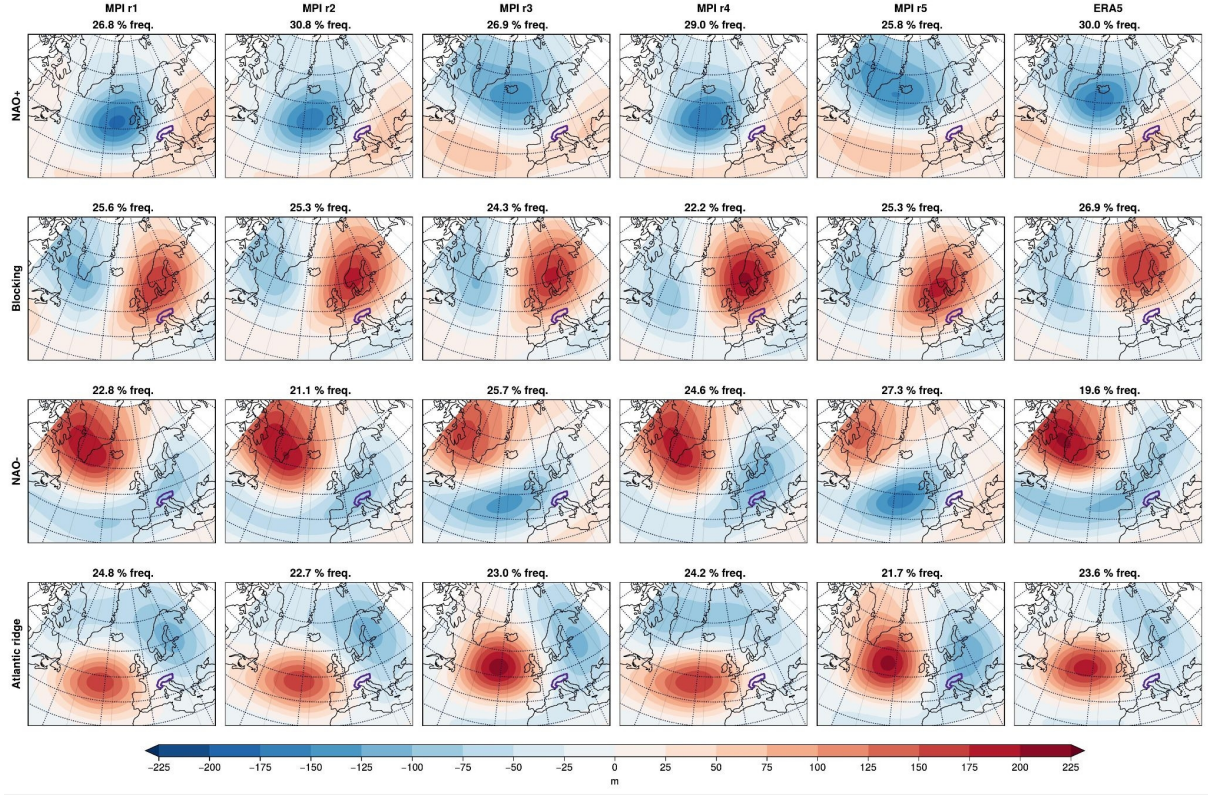
Figure A1 reveals substantial internal variability in the weather regimes simulated by MPI-ESM1-2-HR. For the NAO+ regime, realizations r1, r2, r4, r6, r7, and r10 exhibit a southward displacement of the low-pressure center relative to ERA5. By contrast, realizations r3, r5, r8, and r9 reproduce the ERA5 pattern more closely. The Blocking regime displays comparatively less variability, although noticeable differences remain. When larger biases occur, they generally correspond to a southwestward displacement of the anticyclonic center (e.g. r1, r5, r6, and r10).

The NAO- regime exhibits considerable variability among realizations. In particular, realizations r3, r5, and r9 show a weaker extension of the cyclonic center towards the southeastern Atlantic, accompanied by a stronger low-pressure center near the European coastline. The Atlantic Ridge regime also displays pronounced variability. Realizations r3, r5, and r9 exhibit a marked northwestward extension of the anticyclonic center, whereas r4, r6, and r10 show a flatter and less distinct ridge structure, making the resulting pattern resemble a NAO+ regime more closely than a canonical Atlantic Ridge.

An important feature of Figure A1 is that the variability does not appear entirely random. Similar characteristics often occur simultaneously across several regimes within a given realization. For example, realizations r3, r5, and r9 combine a NAO+ pattern that is relatively close to ERA5 with a weaker NAO- ridge extension and a more pronounced Atlantic Ridge. Conversely, realizations r4, r6, and r10 exhibit both a southward-displaced NAO+ pattern resembling an Atlantic Low configuration and an Atlantic Ridge pattern that approaches a NAO+-like structure.

These results suggest that internal variability affects not only the position and intensity of individual weather regimes but also their relationships to one another. Rather than forming completely distinct and independent circulation states, the regimes appear to occupy a continuum of circulation patterns, with internal variability modulating their exact expression within that continuum.

https://doi.org/10.5194/egusphere-2026-7095
Preprint. Discussion started: 27 November 2026
© Author(s) 2026. CC BY 4.0 License.



725

https://doi.org/10.5194/egusphere-2026-7095
Preprint. Discussion started: 27 November 2026
© Author(s) 2026. CC BY 4.0 License.

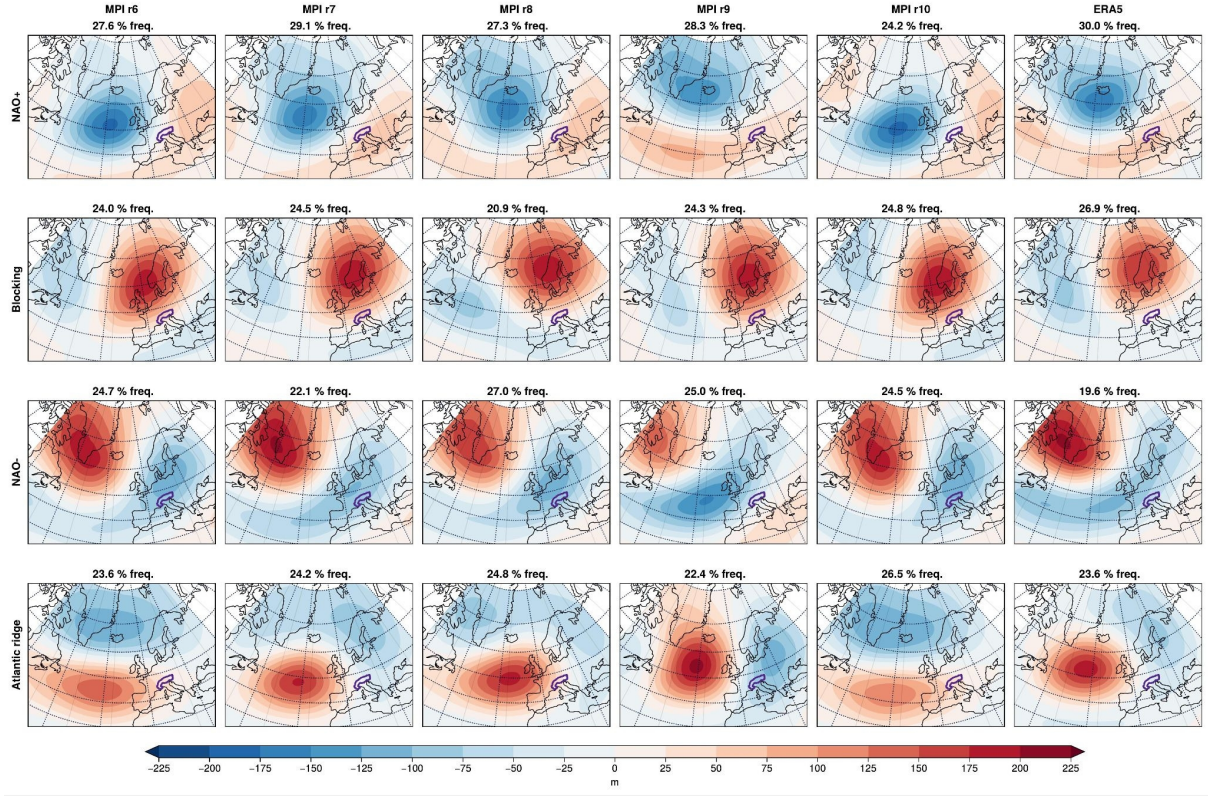


Figure A1: Geopotential height at 500hPa for the four identified weather regimes during winter (NDJFM), 1961-2009. Purple contour shows the Alps. Top: MPI-ESM1-2-HR realisations r1-r5 and ERA5. Bottom: realisations MPI-ESM1-2-HR realisations r6-r10 and ERA5.

B – Historical summer (JJA) weather regimes and precipitation climatology

This appendix presents the summer counterpart to the winter analysis discussed in Sect. 3.1. It examines the relationship between large-scale weather regimes and Alpine precipitation during the historical period (1961–2009). As in the main text, ERA5 is used as a reference dataset for large-scale circulation, while the MAR simulation driven by ERA5 serves as a benchmark against which the GCM-driven MAR simulations are evaluated.

Figure B1 shows the four summer weather regimes identified in ERA5, MPI-ESM1-2-HR (MPI), and EC-Earth3. All four regimes are reproduced sufficiently well to allow a one-to-one correspondence between the models and the reanalysis. Nevertheless, several differences can be identified. For NAO+, the cyclonic center is displaced southwestward in MPI and eastward in EC-Earth3 relative to ERA5. For the Blocking regime, MPI reproduces the position of the anticyclonic center reasonably well, although the ridge is weaker and the associated trough is stronger than in ERA5. In EC-Earth3, the ridge is shifted eastward. The NAO- regime exhibits comparatively small differences between the models and ERA5. For the Atlantic Ridge regime, MPI remains relatively close to the reanalysis, whereas EC-Earth3 displays a more pronounced eastward displacement, placing the ridge center over Great Britain rather than west of the British Isles as in ERA5.

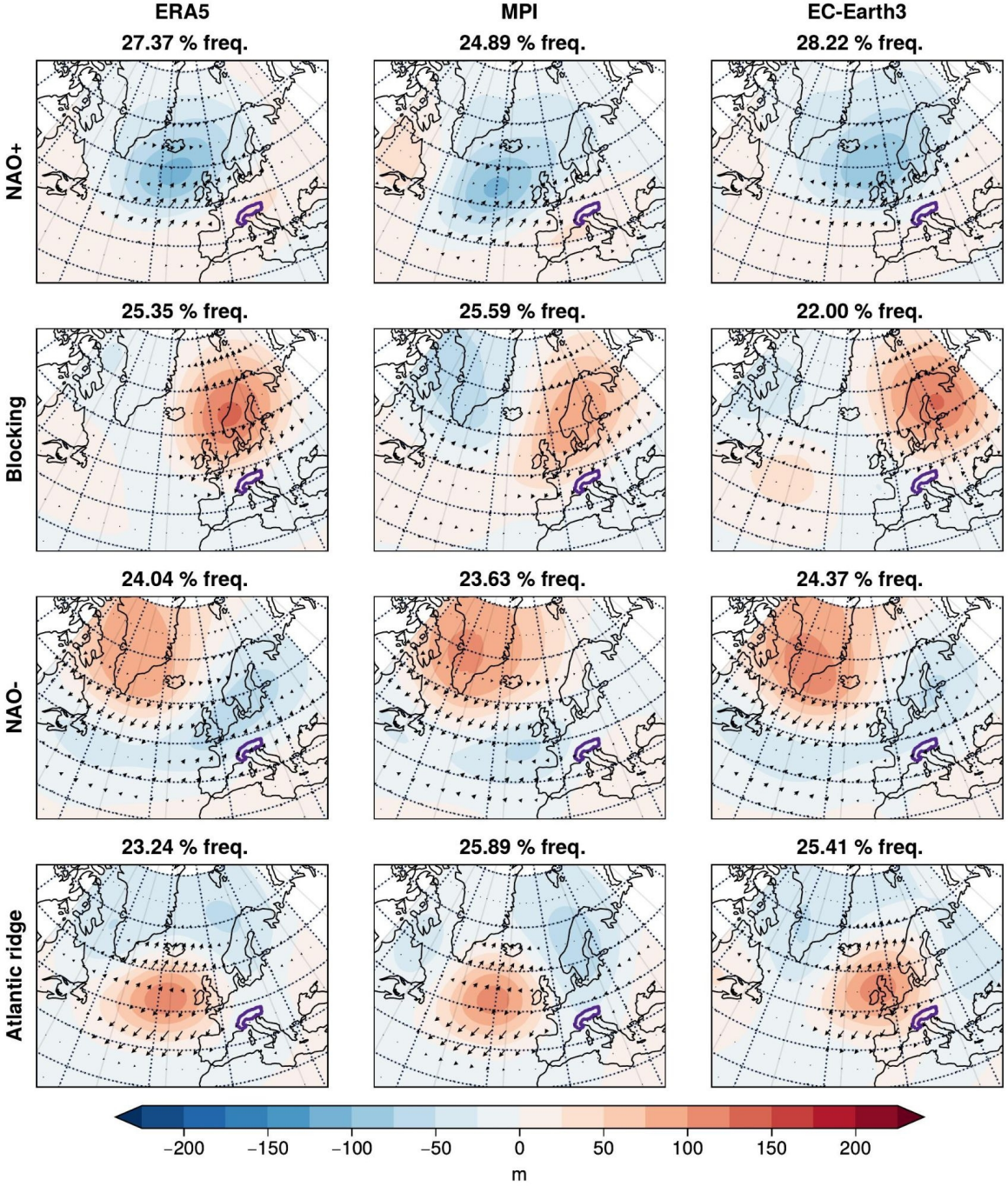
https://doi.org/10.5194/egusphere-2026-7095
Preprint. Discussion started: 27 November 2026
© Author(s) 2026. CC BY 4.0 License.

Figure B2 presents mean summer precipitation and regime-dependent precipitation anomalies in MAR-ERA5. Mean precipitation is generally higher in the northern Alps, where values are around 5 mm day^{-1}, than in the southern Alps, where values are closer to 4 mm day^{-1}. Under NAO+ conditions, precipitation anomalies are predominantly negative across the Alpine region, generally around -10 %. The Blocking regime exhibits a more contrasted pattern, with weak negative anomalies in the north and weak positive anomalies in the south. The NAO- regime is associated with marked spatial contrasts, with positive anomalies reaching 40 % over the northern French and Swiss Alps and negative anomalies approaching -30 % over parts of the southern French and Italian Alps. Under Atlantic Ridge conditions, anomalies remain relatively weak, with slightly negative values in the western Alps and slightly positive values in the eastern Alps.

Figure B3 shows the corresponding results for the MAR-MPI simulation. The spatial structure of the summer climatology is broadly similar to MAR-ERA5, although precipitation amounts are lower overall, with values of approximately 3 mm day^{-1} in the northern Alps and 2 mm day^{-1} in the southern Alps. Regime-dependent anomaly patterns generally resemble those of MAR-ERA5, with some notable differences. The NAO+ regime is associated with a stronger precipitation deficit, locally reaching -30 to -40 %. In addition, the Atlantic Ridge regime exhibits more widespread positive anomalies, particularly over the southern Alps, where values locally reach 30-40 %.

Figure B4 presents the MAR-EC-Earth3 simulation. Aside from mean seasonal precipitation which is closer although still lower, differences relative to MAR-ERA5 are somewhat larger than for MAR-MPI. Under NAO+ conditions, weak positive anomalies appear over the northwestern Alps, whereas most of the region remains characterized by weak negative anomalies. The Blocking regime is associated with widespread positive anomalies, reaching 30-40 % over parts of the southern Alps. The NAO- regime remains broadly similar to MAR-ERA5. The largest discrepancy occurs for the Atlantic Ridge regime, which exhibits widespread negative anomalies across most of the Alpine region, locally exceeding -40 %, with the exception of the southernmost French and Italian Alps. This behaviour is consistent with the eastward displacement of the ridge in EC-Earth3 shown in Figure B1, which places the circulation anomaly closer to the Alpine region.

https://doi.org/10.5194/egusphere-2026-7095
Preprint. Discussion started: 27 November 2026
© Author(s) 2026. CC BY 4.0 License.



765

Figure B1: Geopotential height and winds at 500hPa for summer (JJA), 1961-2009. Purple contour shows the Alps. Left: ERA5 reanalysis; middle: MPI-ESM1-2-HR experiment (r1i1p1f1); right: EC-Earth3 experiment (r25i1p1f1). Rows correspond to the four weather regimes identified in Sect. 2.2.1.

https://doi.org/10.5194/egusphere-2026-7095
Preprint. Discussion started: 27 November 2026
© Author(s) 2026. CC BY 4.0 License.

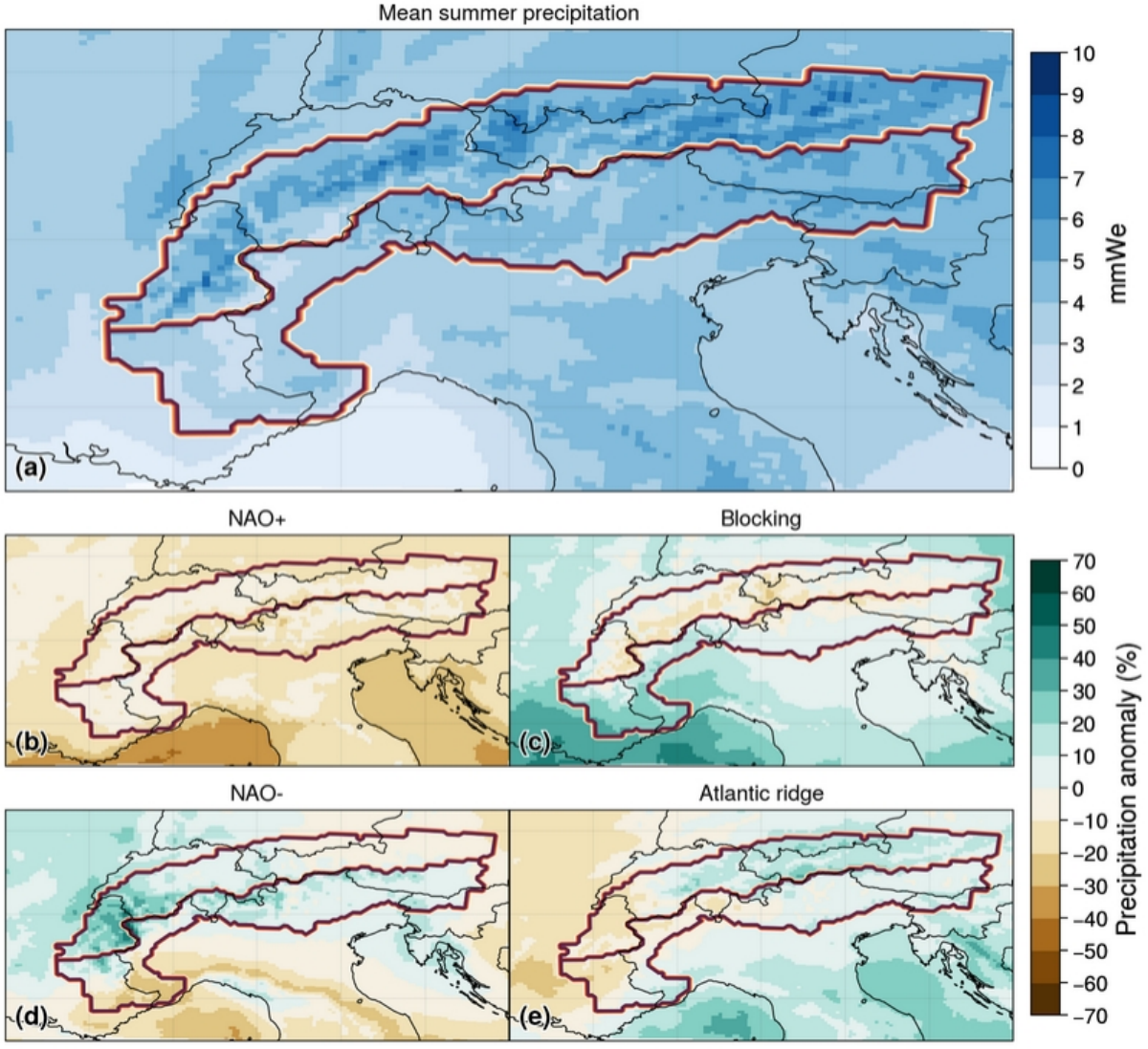


Figure B2: MAR-ERA5 summer precipitation (top) and anomalies by weather regime (bottom) averaged over 1961-2009. The northern and southern boundaries of the Alps as described in Sect. 2.2.2 are superimposed.

https://doi.org/10.5194/egusphere-2026-7095
Preprint. Discussion started: 27 November 2026
© Author(s) 2026. CC BY 4.0 License.

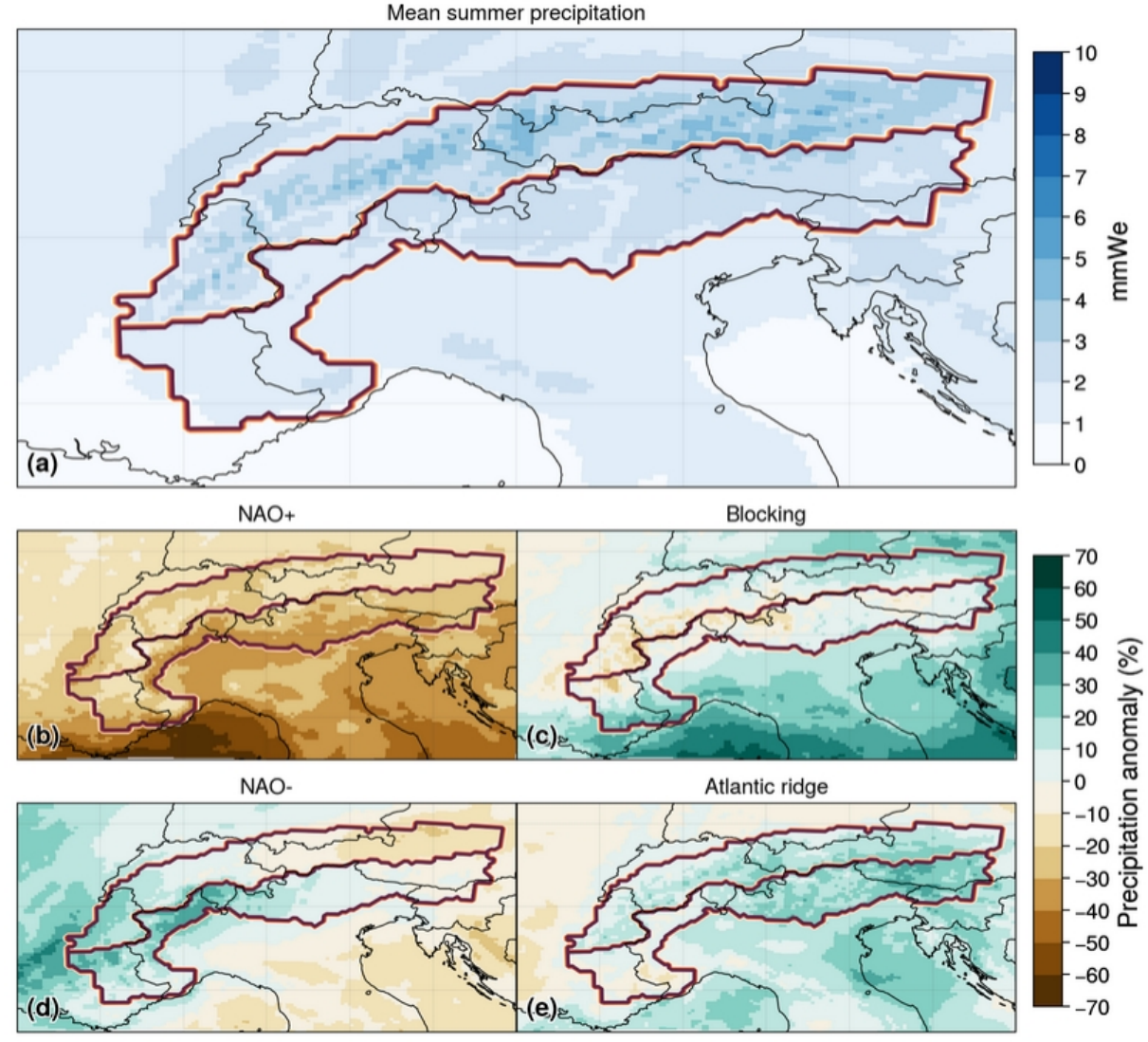


Figure B3: Same as Fig. B2 but for MAR-MPI.

https://doi.org/10.5194/egusphere-2026-7095
Preprint. Discussion started: 27 November 2026
© Author(s) 2026. CC BY 4.0 License.

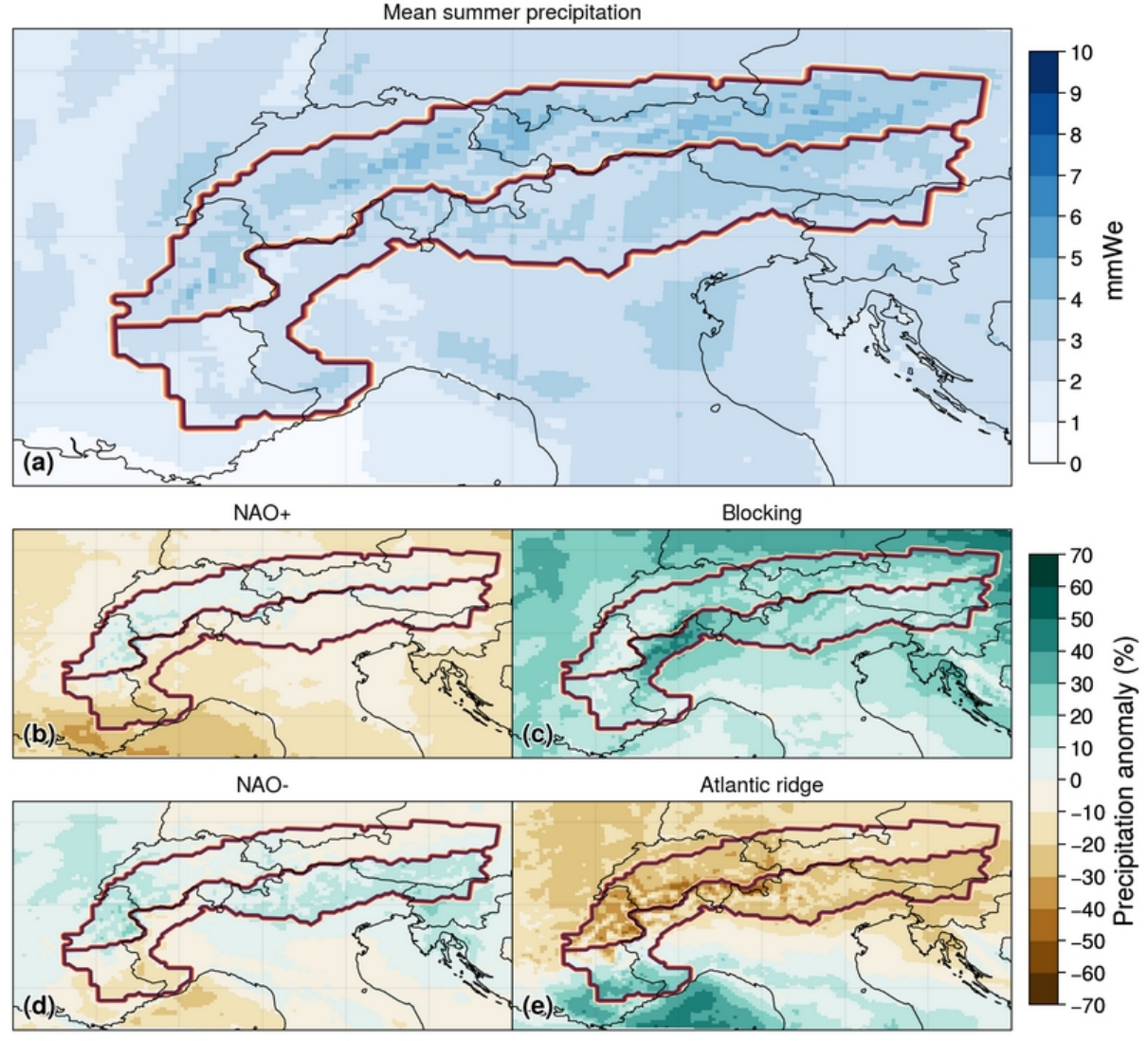


Figure B4: Same as Fig. B2 but for MAR-EC-Earth3.

C – Summer (JJA) projected changes in circulation and precipitation

This appendix presents the summer counterpart to the projected changes discussed in Sect. 3.2.

Figure C1 shows projected changes in large-scale circulation for the three simulations considered in this study. Differences in 500 hPa geopotential height (Z500) anomalies between the projected and historical periods are shown in colour, while the historical climatology is represented by contours and associated wind anomalies by arrows. Regime frequencies are indicated for both periods, together with the Teweles-Wobus (TW) score, which quantifies the similarity between projected and historical circulation patterns (Sect. 2.2.3).

https://doi.org/10.5194/egusphere-2026-7095
Preprint. Discussion started: 27 November 2026
© Author(s) 2026. CC BY 4.0 License.

For the NAO+ regime, projected changes are generally weak and lack consistency across simulations. MPI SSP2-4.5 exhibits a strengthening of the northern part of the cyclonic anomaly and a weakening of its southern flank. MPI SSP5-8.5 shows a west-to-east dipole, with weakening in the western sector and strengthening in the eastern sector. In EC-Earth3, changes are minimal, resulting in the lowest TW score of all summer regimes (0.17).

For the Blocking regime, responses are again heterogeneous. MPI SSP2-4.5 and EC-Earth3 project westward and southwestward displacements of the anticyclonic centre, respectively, whereas MPI SSP5-8.5 is characterized by a more general weakening of the circulation pattern.

For NAO-, both SSP2-4.5 simulations display similar changes, marked by a weakening of the anticyclonic anomaly along its southeastern flank. In MPI SSP5-8.5, the dominant change is instead a southeastward displacement of the circulation pattern.

The Atlantic Ridge regime exhibits the largest structural changes. MPI SSP2-4.5 projects a northward displacement of the ridge, whereas MPI SSP5-8.5 shows a predominantly eastward shift. EC-Earth3 displays a pronounced northwestward displacement, resulting in the highest TW score of the figure (0.41), indicative of substantial changes in the circulation structure relative to the historical period.

Overall, summer TW scores are generally higher than their winter counterparts, suggesting larger changes in circulation structure and supporting the notion that summer weather regimes are less distinct and potentially more sensitive to internal variability than winter regimes.

Figure C2 presents projected summer precipitation changes in MAR-MPI SSP2-4.5. Seasonal mean precipitation decreases across most of the Alpine region by approximately 10-20 %. This signal is primarily associated with strong reductions in precipitation during NAO- conditions, locally exceeding -50 %, and with more moderate decreases during Atlantic Ridge events. By contrast, changes associated with Blocking and NAO+ are spatially more heterogeneous and tend to be weakly positive on average.

Figure C3 shows the corresponding results for MAR-MPI SSP5-8.5. Seasonal mean precipitation again decreases across most of the Alps, although localized areas of weak positive change remain. As in SSP2-4.5, NAO+ is characterized by spatially contrasted but generally positive changes. The Blocking regime differs more substantially, exhibiting predominantly negative changes except at some high-elevation locations. NAO- also shows widespread precipitation decreases, although the magnitude of the signal is slightly weaker than in SSP2-4.5. Despite the contrasting circulation changes simulated for NAO- in Figure C1, both scenarios produce similar precipitation responses. Atlantic Ridge is again associated with a predominantly negative precipitation signal, except in the southernmost Alps, where localized increases exceed 50 %.

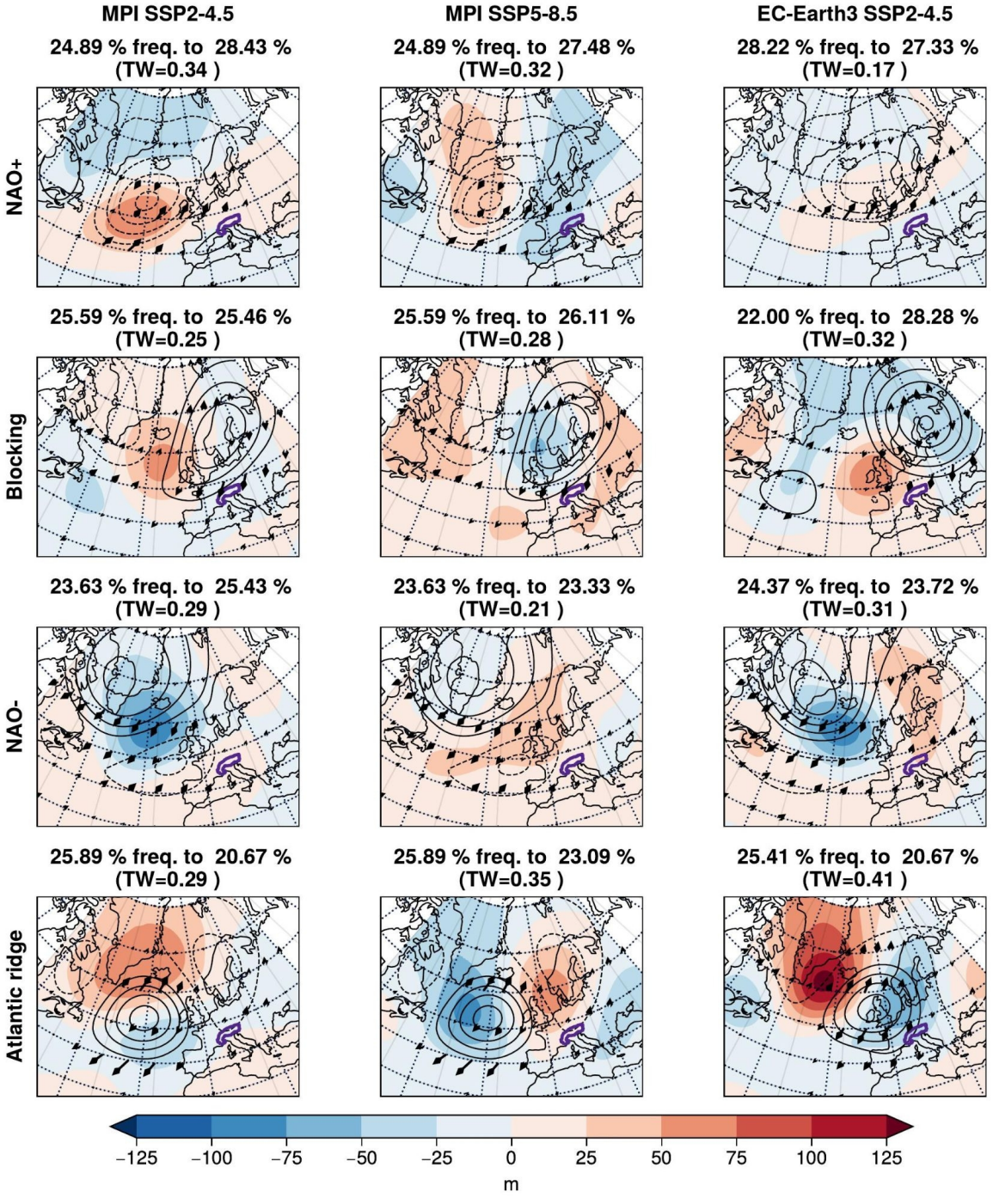
Figure C4 presents projected changes in MAR-EC-Earth3. In contrast to the MPI-driven simulations, seasonal mean precipitation generally increases across the Alps, except in parts of the northern French Alps and Switzerland. A similar

https://doi.org/10.5194/egusphere-2026-7095
Preprint. Discussion started: 27 November 2026
© Author(s) 2026. CC BY 4.0 License.

spatial pattern is found for NAO+ precipitation changes. Under Blocking conditions, precipitation responses are spatially heterogeneous, with positive changes over the southern Alps and weaker, patchier signals elsewhere. The NAO- regime also exhibits heterogeneous behaviour, although negative changes dominate over much of the region, consistent with the decreases simulated in the MPI experiments. Finally, the Atlantic Ridge regime displays the strongest differences relative to the MPI simulations, with widespread positive changes over high-elevation regions and the Italian Alps, locally exceeding 50 %, alongside weaker and more spatially variable signals elsewhere. This behaviour is consistent with the substantial circulation changes associated with this regime in Figure C1.

Taken together, the summer projections reveal a greater diversity of circulation and precipitation responses than those found in winter. While NAO- consistently exhibits reduced precipitation across all simulations, the response of the other regimes depends strongly on the driving GCM and scenario.

https://doi.org/10.5194/egusphere-2026-7095
Preprint. Discussion started: 27 November 2026
© Author(s) 2026. CC BY 4.0 License.



825 **Figure C1: Difference in summer (JJA) geopotential height between projection and historical period (shading). Geopotential height and wind climatology for the historical period are shown with isolines and arrows respectively. Solid lines indicate positive values and dashed lines indicate negative values, with a contour interval of 25 m.**

https://doi.org/10.5194/egusphere-2026-7095
Preprint. Discussion started: 27 November 2026
© Author(s) 2026. CC BY 4.0 License.

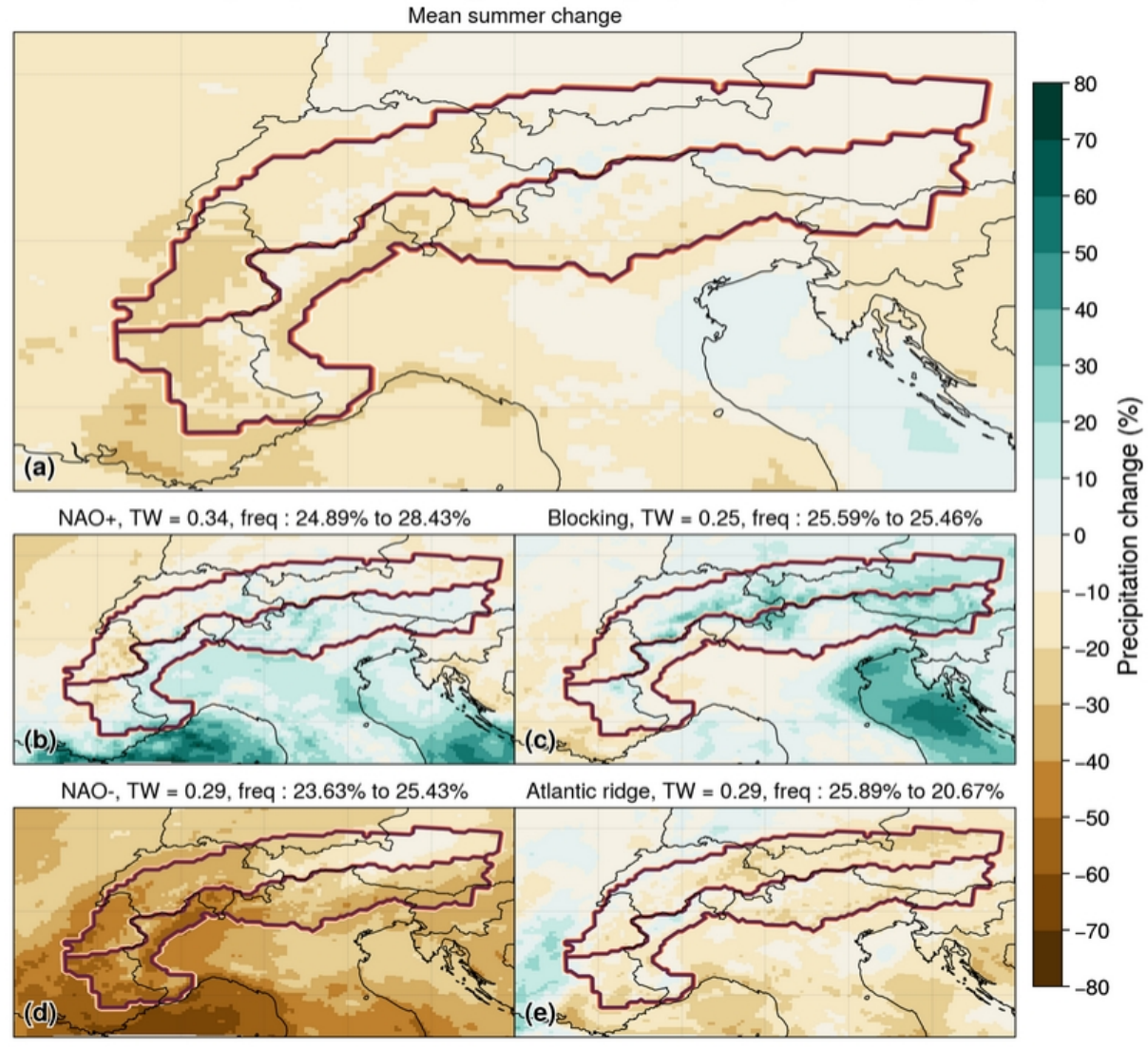


Figure C2: MAR-MPI summer (JJA) precipitation changes between projection (SSP2-4.5, 2050-2099) and historic period (1961-2009), by weather regime. The Teweles-Wobus score between the two periods for each weather regime is given, as well as the frequency changes for each weather regime.

https://doi.org/10.5194/egusphere-2026-7095
Preprint. Discussion started: 27 November 2026
© Author(s) 2026. CC BY 4.0 License.

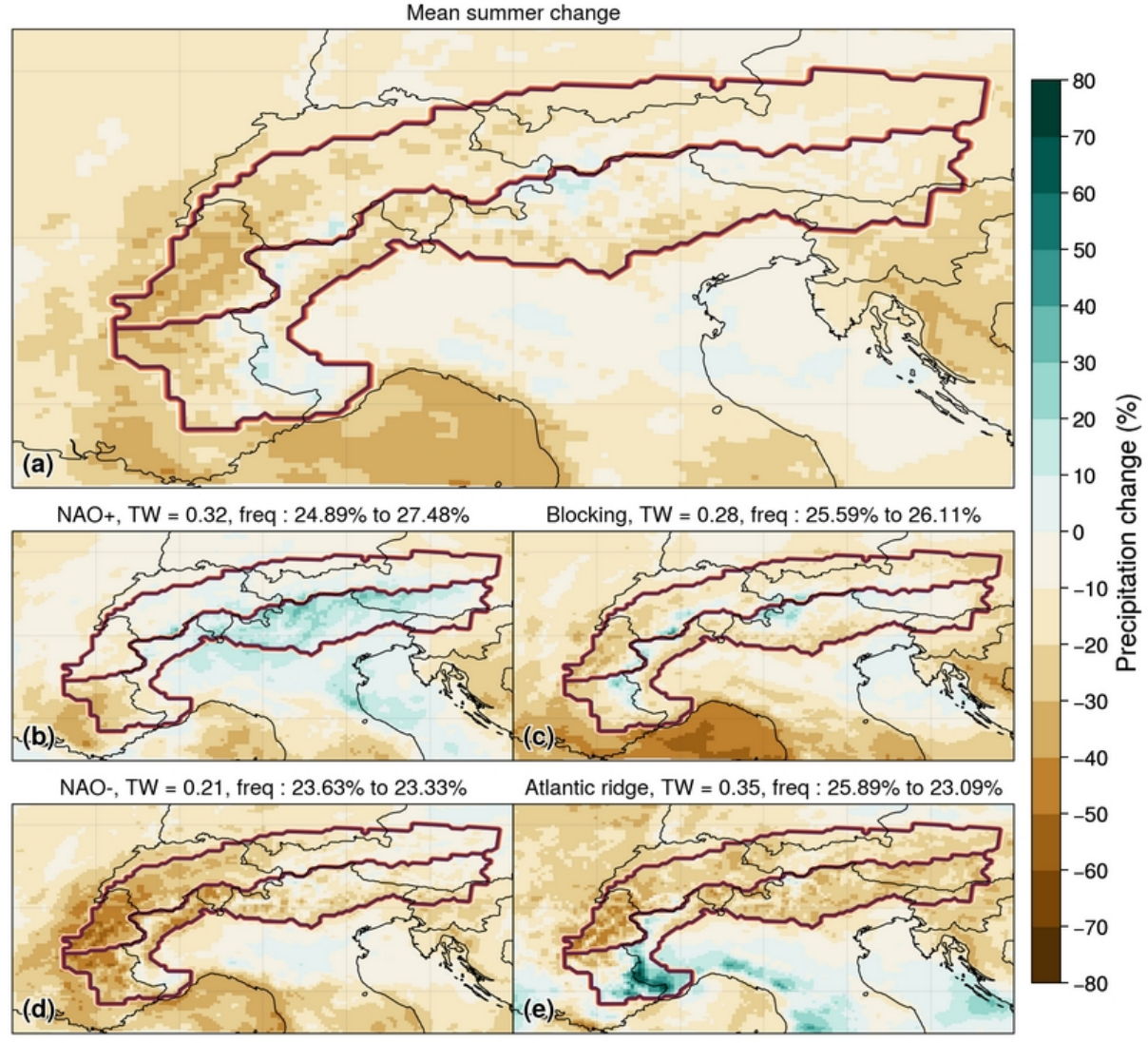


Figure C3: Same as Fig. C2 but for MAR-MPI SSP5-8.5.

https://doi.org/10.5194/egusphere-2026-7095
Preprint. Discussion started: 27 November 2026
© Author(s) 2026. CC BY 4.0 License.

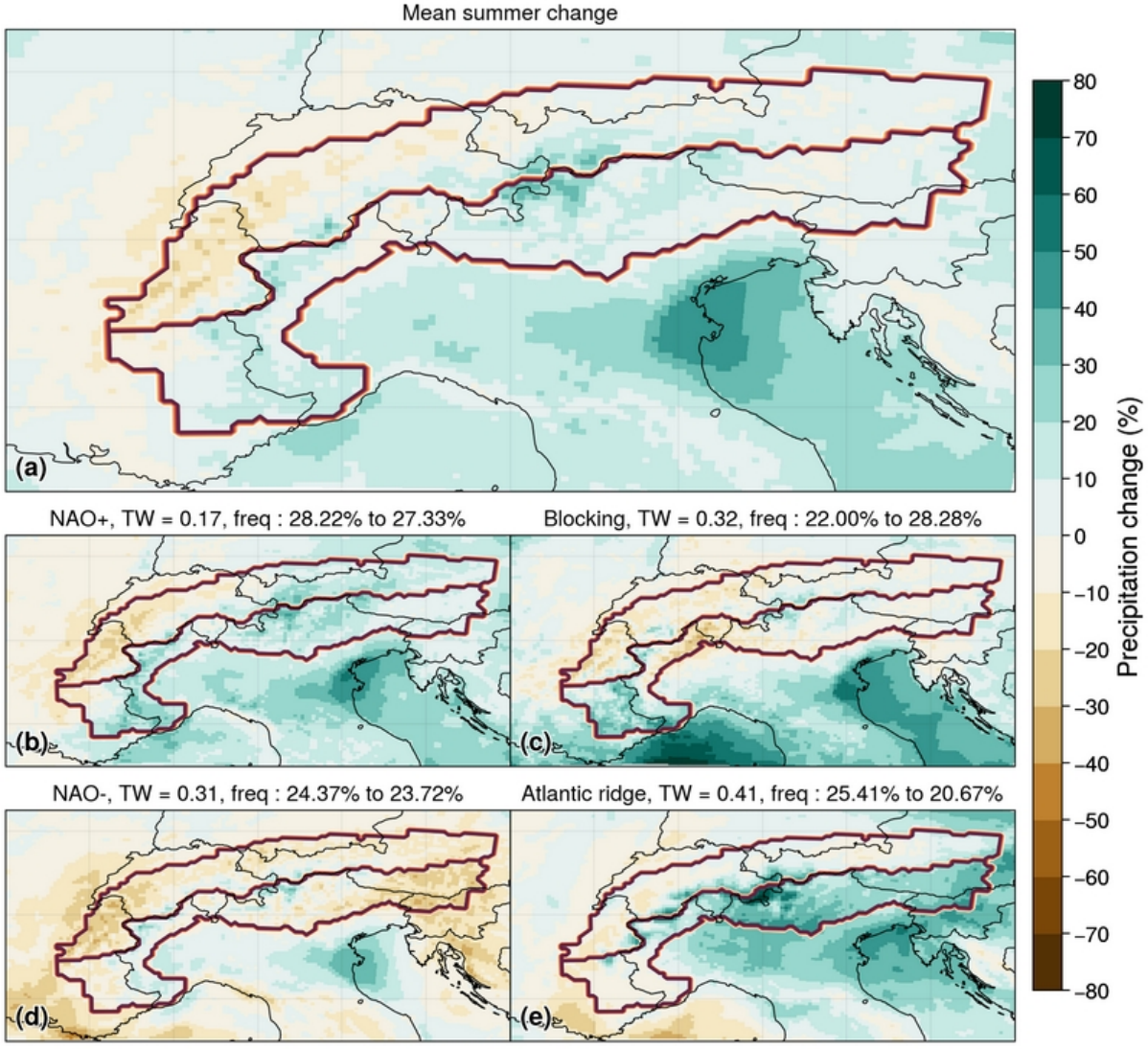


Figure C4: Same as Fig. C2 but for MAR-EC-Earth3 SSP2-4.5.

Code and data availability

All scripts to produce the figures are available at https://github.com/Ian-CD/PhD/tree/master/Precip_weather_types. The Python environment used is also included.

The MAR simulations are available on Zenodo repositories.

Version 3.10: Beaumet et al., 2022a (https://doi.org/10.5281/zenodo.5834221), Beaumet et al., 2022b (https://doi.org/10.5281/zenodo.5834376), Beaumet et al., 2022c (https://doi.org/10.5281/zenodo.5838345)

Version 3.14: Castellanos et al., 2026a (https://doi.org/10.5281/zenodo.21047278).

https://doi.org/10.5194/egusphere-2026-7095
Preprint. Discussion started: 27 November 2026
© Author(s) 2026. CC BY 4.0 License.

The GCM and ERA5 data was downloaded from the IPSL Data and Computing Center ESPRI.

Author contributions

MM and JBe produced the MAR version 3.10 simulations. IC produced the MAR version 3.14 simulation, with help from MC. SB provided methods and scripts helpful to conduct the study. XF developed MAR and provided helpful discussion and information on the model. EM-C provided the EC-Earth3 forcing files. JBe, MM and JBl contributed to the design and the direction of the study. IC produced the figures and wrote the article, and all authors contributed with suggested changes and helpful comments.

Competing interests

The contact author has declared that none of the authors has any competing interests.

Acknowledgements

The authors thank María Santolaria-Otín for helpful discussions on weather regimes. To access the general circulation model data, this study also benefited from the IPSL mesocenter ESPRI facility which is supported by CNRS, UPMC, Labex L-IPSL, CNES and Ecole Polytechnique. All (or most of) the computations presented in this paper were performed using the GRICAD infrastructure (https://gricad.univ-grenoble-alpes.fr), which is supported by Grenoble research communities.

References

Auer, I., Böhm, R., Jurkovic, A., Lipa, W., Orlik, A., Potzmann, R., Schöner, W., Ungersböck, M., Matulla, C., Briffa, K., Jones, P., Efthymiadis, D., Brunetti, M., Nanni, T., Maugeri, M., Mercalli, L., Mestre, O., Moisselin, J., Begert, M., Müller-Westermeier, G., Kveton, V., Bochnicek, O., Stastny, P., Lapin, M., Szalai, S., Szentimrey, T., Cegnar, T., Dolinar, M., Gajic-Capka, M., Zaninovic, K., Majstorovic, Z., and Nieplova, E.: HISTALP—historical instrumental climatological surface time series of the Greater Alpine Region, Intl Journal of Climatology, 27, 17–46, https://doi.org/10.1002/joc.1377, 2007.

Babanov, B. A., Semenov, V. A., and Mokhov, I. I.: Comparison of Cluster Analysis Methods for Identifying Weather Regimes in the Euro-Atlantic Region for Winter and Summer Seasons, Izv. Atmos. Ocean. Phys., 59, 605–623, https://doi.org/10.1134/S0001433823060026, 2023.

Bacer, S., Jomaa, F., Beaumet, J., Gallée, H., Le Bouëdec, E., Ménégoz, M., and Staquet, C.: Impact of climate change on wintertime European atmospheric blocking, Weather and Climate Dynamics, 3, 377–389, https://doi.org/10.5194/wcd-3-377-2022, 2022.

https://doi.org/10.5194/egusphere-2026-7095
Preprint. Discussion started: 27 November 2026
© Author(s) 2026. CC BY 4.0 License.

Bacer, S., Beaumet, J., Ménégoz, M., Gallée, H., Le Bouëdec, E., and Staquet, C.: Impact of climate change on persistent cold-air pools in an alpine valley during the 21st century, Weather and Climate Dynamics, 5, 211–229, https://doi.org/10.5194/wcd-5-211-2024, 2024.

Ban, N., Schmidli, J., and Schär, C.: Heavy precipitation in a changing climate: Does short-term summer precipitation increase faster?, Geophysical Research Letters, 42, 1165–1172, https://doi.org/10.1002/2014GL062588, 2015.

Beaumet, J., Ménégoz, M., Morin, S., Gallée, H., Fettweis, X., Six, D., Vincent, C., Wilhelm, B., and Anquetin, S.: Twentieth century temperature and snow cover changes in the French Alps, Reg Environ Change, 21, 114, https://doi.org/10.1007/s10113-021-01830-x, 2021.

Beaumet, J., Menegoz, M., Gallée, H., and Chamarro, E. M.: MAR-EC-Earth3 HIST (1961-2014) and SSP245 European Alps (2015-2100), https://doi.org/10.5281/zenodo.5838345, 2022a.

Beaumet, J., Menegoz, M., and Gallée, H.: MAR-MPI-ESM1-2-HR SSP585 European Alps (2015-2100), https://doi.org/10.5281/zenodo.5834376, 2022b.

Beaumet, J., Menegoz, M., and Gallée, H.: MAR-MPI-ESM1-2-HR HIST (1961-2014) and SSP245 European Alps (2015-2100), https://doi.org/10.5281/zenodo.5834221, n.d.

Beck, C., Jacobeit, J., and Jones, P. D.: Frequency and within-type variations of large-scale circulation types and their effects on low-frequency climate variability in central europe since 1780, International Journal of Climatology, 27, 473–491, https://doi.org/10.1002/joc.1410, 2007.

Ben Daoud, A., Sauquet, E., Bontron, G., Obled, C., and Lang, M.: Daily quantitative precipitation forecasts based on the analogue method: Improvements and application to a French large river basin, Atmospheric Research, 169, 147–159, https://doi.org/10.1016/j.atmosres.2015.09.015, 2016.

Blanc, A., Blanchet, J., and Creutin, J.: Past evolution of western Europe large-scale circulation and link to precipitation trend in the northern French Alps, Weather and Climate Dynamics, 3, 231–250, https://doi.org/10.5194/wcd-3-231-2022, 2022.

Blanchet, J., Blanc, A., and Creutin, J.-D.: Explaining recent trends in extreme precipitation in the Southwestern Alps by changes in atmospheric influences, Weather and Climate Extremes, 33, 100356, https://doi.org/10.1016/j.wace.2021.100356, 2021a.

Blanchet, J., Creutin, J.-D., and Blanc, A.: Retreating winter and strengthening autumn Mediterranean influence on extreme precipitation in the Southwestern Alps over the last 60 years, Environ. Res. Lett., 16, 034056, https://doi.org/10.1088/1748-9326/abb5cd, 2021b.

Boé, J., Terray, L., Cassou, C., and Najac, J.: Uncertainties in European summer precipitation changes: role of large scale circulation, Clim Dyn, 33, 265–276, https://doi.org/10.1007/s00382-008-0474-7, 2009.

Böhnisch, A., Ludwig, R., and Leduc, M.: Using a nested single-model large ensemble to assess the internal variability of the North Atlantic Oscillation and its climatic implications for central Europe, Earth System Dynamics, 11, 617–640, https://doi.org/10.5194/esd-11-617-2020, 2020.

Bracegirdle, T. J.: Early-to-Late Winter 20th Century North Atlantic Multidecadal Atmospheric Variability in Observations, CMIP5 and CMIP6, Geophysical Research Letters, 49, e2022GL098212, https://doi.org/10.1029/2022GL098212, 2022.

https://doi.org/10.5194/egusphere-2026-7095
Preprint. Discussion started: 27 November 2026
© Author(s) 2026. CC BY 4.0 License.

Brönnimann, S., Rajczak, J., Fischer, E. M., Raible, C. C., Rohrer, M., and Schär, C.: Changing seasonality of moderate and extreme precipitation events in the Alps, Natural Hazards and Earth System Sciences, 18, 2047–2056, https://doi.org/10.5194/nhess-18-2047-2018, 2018.

Brönnimann, S., Franke, J., Valler, V., Hand, R., Samakinwa, E., Lundstad, E., Burgdorf, A.-M., Lipfert, L., Pfister, L., Imfeld, N., and Rohrer, M.: Past hydroclimate extremes in Europe driven by Atlantic jet stream and recurrent weather patterns, Nat. Geosci., 18, 246–253, https://doi.org/10.1038/s41561-025-01654-y, 2025.

Brunetti, M., Maugeri, M., Nanni, T., Auer, I., Böhm, R., and Schöner, W.: Precipitation variability and changes in the greater Alpine region over the 1800–2003 period, Journal of Geophysical Research: Atmospheres, 111, https://doi.org/10.1029/2005JD006674, 2006.

Çalışır, E., Amarouche, K., Çakmak, R. E., and Akpınar, A.: Performance assessment of 22 CMIP6 climate models for projecting wind climate and wind power over the Mediterranean Sea, Environ Earth Sci, 85, 170, https://doi.org/10.1007/s12665-026-12885-6, 2026.

Cannon, A. J.: Reductions in daily continental-scale atmospheric circulation biases between generations of global climate models: CMIP5 to CMIP6, Environ. Res. Lett., 15, 064006, https://doi.org/10.1088/1748-9326/ab7e4f, 2020.

Castellanos, I., Ménégoz, M., and Gallée, H.: MARv3.14-ERA5 HIST European Alps (1940-2025), https://doi.org/10.5281/zenodo.21047278, 2026a.

Castellanos, I., Ménégoz, M., Blanchet, J., Beaumet, J., Gallée, H., Moreno-Chamarro, E., Staquet, C., and Fettweis, X.: Projected elevation-dependent warming in the Alps: contrasting free-atmosphere and surface trends with surface energy balance drivers, Earth System Dynamics, 17, 581–605, https://doi.org/10.5194/esd-17-581-2026, 2026b.

Coppola, E., Nogherotto, R., Ciarlo', J. M., Giorgi, F., van Meijgaard, E., Kadygrov, N., Iles, C., Corre, L., Sandstad, M., Somot, S., Nabat, P., Vautard, R., Levavasseur, G., Schwingshackl, C., Sillmann, J., Kjellström, E., Nikulin, G., Aalbers, E., Lenderink, G., Christensen, O. B., Boberg, F., Sørland, S. L., Demory, M.-E., Bülow, K., Teichmann, C., Warrach-Sagi, K., and Wulfmeyer, V.: Assessment of the European Climate Projections as Simulated by the Large EURO-CORDEX Regional and Global Climate Model Ensemble, Journal of Geophysical Research: Atmospheres, 126, e2019JD032356, https://doi.org/10.1029/2019JD032356, 2021.

Cortesi, N., Torralba, V., González-Reviriego, N., Soret, A., and Doblas-Reyes, F. J.: Characterization of European wind speed variability using weather regimes, Clim Dyn, 53, 4961–4976, https://doi.org/10.1007/s00382-019-04839-5, 2019.

Cortesi, N., Torralba, V., Lledó, L., Manrique-Suñén, A., Gonzalez-Reviriego, N., Soret, A., and Doblas-Reyes, F. J.: Yearly evolution of Euro-Atlantic weather regimes and of their sub-seasonal predictability, Clim Dyn, 56, 3933–3964, https://doi.org/10.1007/s00382-021-05679-y, 2021.

Cusinato, E., Rubino, A., and Zanchettin, D.: Winter Euro-Atlantic Climate Modes: Future Scenarios From a CMIP6 Multi-Model Ensemble, Geophysical Research Letters, 48, e2021GL094532, https://doi.org/10.1029/2021GL094532, 2021.

Dolores-Tesillos, E., Martius, O., and Quinting, J.: On the role of moist and dry processes in atmospheric blocking biases in the Euro-Atlantic region in CMIP6, Weather and Climate Dynamics, 6, 471–487, https://doi.org/10.5194/wcd-6-471-2025, 2025.

Döscher, R., Acosta, M., Alessandri, A., Anthoni, P., Arsouze, T., Bergman, T., Bernardello, R., Boussetta, S., Caron, L.-P., Carver, G., Castrillo, M., Catalano, F., Cvijanovic, I., Davini, P., Dekker, E., Doblas-Reyes, F. J., Docquier, D., Echevarria,

https://doi.org/10.5194/egusphere-2026-7095
Preprint. Discussion started: 27 November 2026
© Author(s) 2026. CC BY 4.0 License.

P., Fladrich, U., Fuentes-Franco, R., Gröger, M., v. Hardenberg, J., Hieronymus, J., Karami, M. P., Keskinen, J.-P., Koenigk, T., Makkonen, R., Massonnet, F., Ménégoz, M., Miller, P. A., Moreno-Chamarro, E., Nieradzik, L., van Noije, T., Nolan, P., O'Donnell, D., Ollinaho, P., van den Oord, G., Ortega, P., Prims, O. T., Ramos, A., Reerink, T., Rousset, C., Ruprich-Robert, Y., Le Sager, P., Schmith, T., Schrödner, R., Serva, F., Sicardi, V., Sloth Madsen, M., Smith, B., Tian, T., Tourigny, E., Uotila, P., Vancoppenolle, M., Wang, S., Wårlind, D., Willén, U., Wyser, K., Yang, S., Yepes-Arbós, X., and Zhang, Q.: The EC-Earth3 Earth system model for the Coupled Model Intercomparison Project 6, Geoscientific Model Development, 15, 2973–3020, https://doi.org/10.5194/gmd-15-2973-2022, 2022.

Efthymiadis, D., Jones, P. D., Briffa, K. R., Böhm, R., and Maugeri, M.: Influence of large-scale atmospheric circulation on climate variability in the Greater Alpine Region of Europe, Journal of Geophysical Research: Atmospheres, 112, https://doi.org/10.1029/2006JD008021, 2007.

Evin, G., Somot, S., and Hingray, B.: Balanced estimate and uncertainty assessment of European climate change using the large EURO-CORDEX regional climate model ensemble, Earth System Dynamics, 12, 1543–1569, https://doi.org/10.5194/esd-12-1543-2021, 2021.

Eyring, V., Bony, S., Meehl, G. A., Senior, C. A., Stevens, B., Stouffer, R. J., and Taylor, K. E.: Overview of the Coupled Model Intercomparison Project Phase 6 (CMIP6) experimental design and organization, Geoscientific Model Development, 9, 1937–1958, https://doi.org/10.5194/gmd-9-1937-2016, 2016.

Fabiano, F., Christensen, H. M., Strommen, K., Athanasiadis, P., Baker, A., Schiemann, R., and Corti, S.: Euro-Atlantic weather Regimes in the PRIMAVERA coupled climate simulations: impact of resolution and mean state biases on model performance, Clim Dyn, 54, 5031–5048, https://doi.org/10.1007/s00382-020-05271-w, 2020.

Fabiano, F., Meccia, V. L., Davini, P., Ghinassi, P., and Corti, S.: A regime view of future atmospheric circulation changes in northern mid-latitudes, Weather and Climate Dynamics, 2, 163–180, https://doi.org/10.5194/wcd-2-163-2021, 2021.

Fernandez-Granja, J. A., Casanueva, A., Bedia, J., and Fernandez, J.: Improved atmospheric circulation over Europe by the new generation of CMIP6 earth system models, Clim Dyn, 56, 3527–3540, https://doi.org/10.1007/s00382-021-05652-9, 2021.

Fuentes-Franco, R., Docquier, D., Koenigk, T., Zimmermann, K., and Giorgi, F.: Winter heavy precipitation events over Northern Europe modulated by a weaker NAO variability by the end of the 21st century, npj Clim Atmos Sci, 6, 72, https://doi.org/10.1038/s41612-023-00396-1, 2023.

Gutiérrez, C., Molina, M., Ortega, M., López-Franca, N., and Sánchez, E.: Low-wind climatology (1979–2018) over Europe from ERA5 reanalysis, Clim Dyn, 62, 4155–4170, https://doi.org/10.1007/s00382-024-07123-3, 2024.

Halifa-Marín, A., Torres-Vázquez, M. A., Trigo, R., Vicente-Serrano, S. M., Turco, M., Jiménez-Guerrero, P., and Montávez, J. P.: Too-stable North Atlantic climate system in CMIP6 experiments undermines precipitation projections in Europe, Quarterly Journal of the Royal Meteorological Society, 151, e4999, https://doi.org/10.1002/qj.4999, 2025.

Harvey, B. J., Cook, P., Shaffrey, L. C., and Schiemann, R.: The Response of the Northern Hemisphere Storm Tracks and Jet Streams to Climate Change in the CMIP3, CMIP5, and CMIP6 Climate Models, Journal of Geophysical Research: Atmospheres, 125, e2020JD032701, https://doi.org/10.1029/2020JD032701, 2020.

Hersbach, H., Bell, B., Berrisford, P., Hirahara, S., Horányi, A., Muñoz-Sabater, J., Nicolas, J., Peubey, C., Radu, R., Schepers, D., Simmons, A., Soci, C., Abdalla, S., Abellan, X., Balsamo, G., Bechtold, P., Biavati, G., Bidlot, J., Bonavita,

https://doi.org/10.5194/egusphere-2026-7095
Preprint. Discussion started: 27 November 2026
© Author(s) 2026. CC BY 4.0 License.

M., De Chiara, G., Dahlgren, P., Dee, D., Diamantakis, M., Dragani, R., Flemming, J., Forbes, R., Fuentes, M., Geer, A., Haimberger, L., Healy, S., Hogan, R. J., Hólm, E., Janisková, M., Keeley, S., Laloyaux, P., Lopez, P., Lupu, C., Radnoti, G., de Rosnay, P., Rozum, I., Vamborg, F., Villaume, S., and Thépaut, J.-N.: The ERA5 global reanalysis, Quarterly Journal of the Royal Meteorological Society, 146, 1999–2049, https://doi.org/10.1002/qj.3803, 2020.

Hertig, E. and Jacobeit, J.: Variability of weather regimes in the North Atlantic-European area: past and future, Atmospheric Science Letters, 15, 314–320, https://doi.org/10.1002/asl2.505, 2014.

Hochman, A., Messori, G., Quinting, J. F., Pinto, J. G., and Grams, C. M.: Do Atlantic-European Weather Regimes Physically Exist?, Geophysical Research Letters, 48, e2021GL095574, https://doi.org/10.1029/2021GL095574, 2021.

Ibebuchi, C. C.: On the representation of atmospheric circulation modes in regional climate models over Western Europe, International Journal of Climatology, 43, 668–682, https://doi.org/10.1002/joc.7807, 2023.

Isotta, F. A., Frei, C., Weilguni, V., Perčec Tadić, M., Lassègues, P., Rudolf, B., Pavan, V., Cacciamani, C., Antolini, G., Ratto, S. M., Munari, M., Micheletti, S., Bonati, V., Lussana, C., Ronchi, C., Panettieri, E., Marigo, G., and Vertačnik, G.: The climate of daily precipitation in the Alps: development and analysis of a high-resolution grid dataset from pan-Alpine rain-gauge data, International Journal of Climatology, 34, 1657–1675, https://doi.org/10.1002/joc.3794, 2014.

Jaiser, R., Dethloff, K., Handorf, D., and Cohen, J.: Impact of sea ice cover changes on the Northern Hemisphere atmospheric winter circulation, Tellus, 64, https://doi.org/10.3402/tellusa.v64i0.11595, 2012.

Kotlarski, S., Lüthi, D., and Schär, C.: The elevation dependency of 21st century European climate change: an RCM ensemble perspective, International Journal of Climatology, 35, 3902–3920, https://doi.org/10.1002/joc.4254, 2015.

Laurila, T. K., Sinclair, V. A., and Gregow, H.: Climatology, variability, and trends in near-surface wind speeds over the North Atlantic and Europe during 1979–2018 based on ERA5, International Journal of Climatology, 41, 2253–2278, https://doi.org/10.1002/joc.6957, 2021.

Lavaysse, C., Vogt, J., Toreti, A., Carrera, M. L., and Pappenberger, F.: On the use of weather regimes to forecast meteorological drought over Europe, Natural Hazards and Earth System Sciences, 18, 3297–3309, https://doi.org/10.5194/nhess-18-3297-2018, 2018.

Masson, D. and Frei, C.: Long-term variations and trends of mesoscale precipitation in the Alps: recalculation and update for 1901–2008, International Journal of Climatology, 36, 492–500, https://doi.org/10.1002/joc.4343, 2016.

Matiu, M., Napoli, A., Kotlarski, S., Zardi, D., Bellin, A., and Majone, B.: Elevation-dependent biases of raw and bias-adjusted EURO-CORDEX regional climate models in the European Alps, Clim Dyn, 62, 9013–9030, https://doi.org/10.1007/s00382-024-07376-y, 2024.

Mauritsen, T., Bader, J., Becker, T., Behrens, J., Bittner, M., Brokopf, R., Brovkin, V., Claussen, M., Crueger, T., Esch, M., Fast, I., Fiedler, S., Fläschner, D., Gayler, V., Giorgetta, M., Goll, D. S., Haak, H., Hagemann, S., Hedemann, C., Hohenegger, C., Ilyina, T., Jahns, T., Jimenéz-de-la-Cuesta, D., Jungclaus, J., Kleinen, T., Kloster, S., Kracher, D., Kinne, S., Kleberg, D., Lasslop, G., Kornblueh, L., Marotzke, J., Matei, D., Meraner, K., Mikolajewicz, U., Modali, K., Möbis, B., Müller, W. A., Nabel, J. E. M. S., Nam, C. C. W., Notz, D., Nyawira, S.-S., Paulsen, H., Peters, K., Pincus, R., Pohlmann, H., Pongratz, J., Popp, M., Raddatz, T. J., Rast, S., Redler, R., Reick, C. H., Rohrschneider, T., Schemann, V., Schmidt, H., Schnur, R., Schulzweida, U., Six, K. D., Stein, L., Stemmler, I., Stevens, B., von Storch, J.-S., Tian, F., Voigt, A., Vrese, P., Wieners, K.-H., Wilkenskjeld, S., Winkler, A., and Roeckner, E.: Developments in the MPI-M Earth System Model version

https://doi.org/10.5194/egusphere-2026-7095
Preprint. Discussion started: 27 November 2026
© Author(s) 2026. CC BY 4.0 License.

1.2 (MPI-ESM1.2) and Its Response to Increasing CO2, Journal of Advances in Modeling Earth Systems, 11, 998–1038, https://doi.org/10.1029/2018MS001400, 2019.

Ménégoz, M., Valla, E., Jourdain, N. C., Blanchet, J., Beaumet, J., Wilhelm, B., Gallée, H., Fettweis, X., Morin, S., and Anquetin, S.: Contrasting seasonal changes in total and intense precipitation in the European Alps from 1903 to 2010, Hydrology and Earth System Sciences, 24, 5355–5377, https://doi.org/10.5194/hess-24-5355-2020, 2020.

Molina, M. O., Gutiérrez, C., and Sánchez, E.: Comparison of ERA5 surface wind speed climatologies over Europe with observations from the HadISD dataset, International Journal of Climatology, 41, 4864–4878, https://doi.org/10.1002/joc.7103, 2021.

Müller, W., Jungclaus, J., Mauritsen, T., Baehr, J., Bittner, M., Budich, R., Bunzel, F., Esch, M., Ghosh, R., Haak, H., Ilyina, T., Kleine, T., Kornblueh, L., Li, H., Modali, K., Notz, D., Pohlmann, H., Roeckner, E., Stemmler, I., and Marotzke, J.: A higher-resolution version of the Max Planck Institute Earth System Model (MPI-ESM 1.2-HR), Journal of Advances in Modeling Earth Systems, 10, https://doi.org/10.1029/2017MS001217, 2018.

Napoli, A., Crespi, A., Ragone, F., Maugeri, M., and Pasquero, C.: Variability of orographic enhancement of precipitation in the Alpine region, Sci Rep, 9, 13352, https://doi.org/10.1038/s41598-019-49974-5, 2019.

Olauson, J.: ERA5: The new champion of wind power modelling?, Renewable Energy, 126, 322–331, https://doi.org/10.1016/j.renene.2018.03.056, 2018.

Philipp, A., Beck, C., Huth, R., and Jacobeit, J.: Development and comparison of circulation type classifications using the COST 733 dataset and software, International Journal of Climatology, 36, 2673–2691, https://doi.org/10.1002/joc.3920, 2016.

Plaut, G. and Simonnet, E.: Large-scale circulation classification, weather regimes, and local climate over France, the Alps and Western Europe, Climate Research, 17, 303–324, https://doi.org/10.3354/cr017303, 2001.

Quadrelli, R., Lazzeri, M., Cacciamani, C., and Tibaldi, S.: Observed winter Alpine precipitation variability and links with large-scale circulation patterns, Clim. Res., 17, 275–284, https://doi.org/10.3354/cr017275, 2001.

Reick, C. H., Raddatz, T., Brovkin, V., and Gayler, V.: Representation of natural and anthropogenic land cover change in MPI-ESM, Journal of Advances in Modeling Earth Systems, 5, 459–482, https://doi.org/10.1002/jame.20022, 2013.

Rivosecchi, A., Bollasina, M. A., and Colfescu, I.: Future changes in the influence of the NAO on Mediterranean winter precipitation extremes in the EC-Earth3 large Ensemble: The prominent role of internal variability, Atmospheric Research, 304, 107391, https://doi.org/10.1016/j.atmosres.2024.107391, 2024.

Rousi, E., Selten, F., Rahmstorf, S., and Coumou, D.: Changes in North Atlantic Atmospheric Circulation in a Warmer Climate Favor Winter Flooding and Summer Drought over Europe, Journal of Climate, 34, 2277–2295, https://doi.org/10.1175/JCLI-D-20-0311.1, 2021.

Rummukainen, M.: Added value in regional climate modeling, WIREs Climate Change, 7, 145–159, https://doi.org/10.1002/wcc.378, 2016.

Schmidli, J., Schmutz, C., Frei, C., Wanner, H., and Schär, C.: Mesoscale precipitation variability in the region of the European Alps during the 20th century, Intl Journal of Climatology, 22, 1049–1074, https://doi.org/10.1002/joc.769, 2002.

Stevens, B., Giorgetta, M., Esch, M., Mauritsen, T., Crueger, T., Rast, S., Salzmann, M., Schmidt, H., Bader, J., Block, K., Brokopf, R., Fast, I., Kinne, S., Kornblueh, L., Lohmann, U., Pincus, R., Reichler, T., and Roeckner, E.: Atmospheric

https://doi.org/10.5194/egusphere-2026-7095
Preprint. Discussion started: 27 November 2026
© Author(s) 2026. CC BY 4.0 License.

component of the MPI-M Earth System Model: ECHAM6, Journal of Advances in Modeling Earth Systems, 5, 146–172, https://doi.org/10.1002/jame.20015, 2013.

Struglia, M. V., Anav, A., Antonelli, M., Calmanti, S., Catalano, F., Dell'Aquila, A., Pichelli, E., and Pisacane, G.: Impact of spatial resolution on multi-scenario WRF-ARW simulations driven by the CMIP6 MPI-ESM1-2-HR global model: a focus on precipitation distribution over Italy, Geoscientific Model Development, 18, 6095–6116, https://doi.org/10.5194/gmd-18-6095-2025, 2025.

Teweles, S. and Wobus, H. B.: Verification of Prognostic Charts, Bulletin of the American Meteorological Society, 35, 455–463, https://doi.org/10.1175/1520-0477-35.10.455, 1954.

Torma, C., Giorgi, F., and Coppola, E.: Added value of regional climate modeling over areas characterized by complex terrain—Precipitation over the Alps, Journal of Geophysical Research: Atmospheres, 120, 3957–3972, https://doi.org/10.1002/2014JD022781, 2015.

Vernay, M., Lafaysse, M., Monteiro, D., Hagenmuller, P., Nheili, R., Samacoïts, R., Verfaillie, D., and Morin, S.: The S2M meteorological and snow cover reanalysis over the French mountainous areas: description and evaluation (1958–2021), Earth System Science Data, 14, 1707–1733, https://doi.org/10.5194/essd-14-1707-2022, 2022.

de Vries, H., Lenderink, G., van der Wiel, K., and van Meijgaard, E.: Quantifying the role of the large-scale circulation on European summer precipitation change, Clim Dyn, 59, 2871–2886, https://doi.org/10.1007/s00382-022-06250-z, 2022.

Wanner, H., Rickli, R., Salvisberg, E., Schmutz, C., and Schüepp, M.: Global climate change and variability and its influence on Alpine climate — concepts and observations, Theor Appl Climatol, 58, 221–243, https://doi.org/10.1007/BF00865022, 1997.